

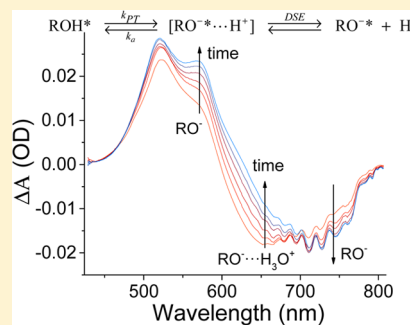
Comprehensive Study of Ultrafast Excited-State Proton Transfer in Water and D₂O Providing the Missing RO⁻...H⁺ Ion-Pair Fingerprint

Ron Simkovitch, Katherine Akulov, Shay Shomer, Michal E. Roth, Doron Shabat, Tal Schwartz, and Dan Huppert*

Raymond and Beverly Sackler Faculty of Exact Sciences, School of Chemistry, Tel Aviv University, Tel Aviv 69978, Israel

S Supporting Information

ABSTRACT: Steady-state and time-resolved optical techniques were employed to study the photoprotolytic mechanism of a general photoacid. Previously, a general scheme was suggested that includes an intermediate product that, up until now, had not been clearly observed experimentally. For our study, we used quinone cyanine 7 (QCy7) and QCy9, the strongest photoacids synthesized so far, to look for the missing intermediate product of an excited-state proton transfer to the solvent. Low-temperature steady-state emission spectra of both QCy7 and QCy9 clearly show an emission band at $T < 165$ K in H₂O ice that could be assigned to ion-pair RO⁻...H₃O⁺, the missing intermediate. Room-temperature femtosecond pump-probe spectroscopy transient spectra at short times ($t < 4$ ps) also shows the existence of transient absorption and emission bands that we assigned to the RO⁻...H₃O⁺ ion pair. The intermediate dissociates on a time scale of 1 ps and about 1.5 ps in H₂O and D₂O samples, respectively.

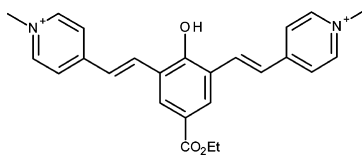


INTRODUCTION

Photoacids are aromatic organic molecules that are weak acids in their ground electronic state, but of acidity greater by many orders of magnitude in their first excited electronic state. Thus, photoexcitation to the excited state, by short UV-vis laser pulses, enables one to follow the photoprotolytic processes. Intermolecular excited-state proton transfer (ESPT) from the acidic group of the excited photoacid to a nearby solvent molecule is widely researched.^{1–16}

In recent studies, we reported on the photoprotolytic properties of a new class of photoacids, the quinone cyanine dyes,^{17,18} and more recently¹⁹ on the photoprotolytic properties of quinone cyanine 9 (QCy9) (shown in Scheme 1)

Scheme 1. Molecular Structure of QCy9



We found that QCy9 is a superphotoacid with $pK_a^* \approx -8.5$; an even more remarkable finding is that it exhibits a very large ESPT rate constant, $k_{PT} \approx 1 \times 10^{13}$ s⁻¹. This is the largest k_{PT} value reported in the literature up to now. For several decades we have used a model that describes the photoprotolytic dissociation of a photoacid and the proton-geminate recombination that may occur subsequently. Below, we briefly describe this model.

REVERSIBLE AND IRREVERSIBLE PHOTOPROTOLYTIC CYCLES OF PHOTOACIDS^{20,21}

Excitation of a photoacid solution of pH lower than its ground-state pK_a generates a vibrationally relaxed, electronically excited ROH molecule (denoted by ROH*) that initiates a photoprotolytic cycle (Scheme 2).

Proton dissociation, with an intrinsic rate constant k_{PT} , leads to the formation of an ion-pair RO⁻...H₃O⁺ that subsequently forms an unpaired RO⁻* and a solvated proton, which diffuses into the bulk of the solvent. The proton and the RO⁻* may recombine via reversible (adiabatic) recombination with a rate constant k_a and re-form the excited acid, ROH*. In general, back-protonation may also proceed by an irreversible (nonadiabatic) pathway, involving fluorescence quenching of the RO⁻* by a proton with a rate constant k_q , forming the ground-state ROH. 1-Naphthol and its derivatives are known to exhibit considerable fluorescence quenching of the deprotonated form, RO⁻, in acidic aqueous solutions.

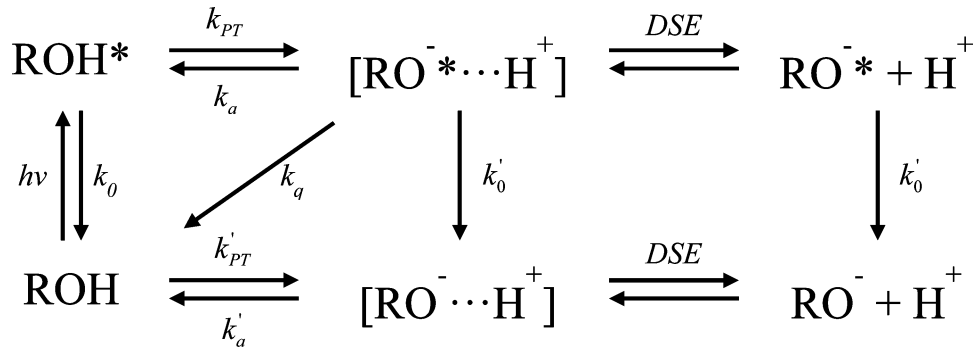
Removal of an ion pair from the contact radius, a , to infinity is described by the transient numerical solution of the Debye-Smoluchowski equation (DSE).^{22,23} The motion of the transferred proton in water near the photoacid depends strongly on the electrical potential existing between it and the deprotonated form. The diffusion-assisted geminate recombination of the RO⁻* with the proton can be quantitatively described with the use of the numerical solution of the DSE under the initial and boundary conditions of the photoprotolytic process. In addition,

Received: January 9, 2014

Revised: May 27, 2014

Published: May 28, 2014

Scheme 2. Photoprotolytic Cycle



the fluorescence lifetimes of all excited species are considered, with $1/k_0 = \tau_{\text{ROH}}$ for the acid, and $1/k_0' = \tau_{\text{RO}^-}$ for the conjugate base. Generally, k_0' and k_0 are much smaller than both the proton-reaction and the diffusion-controlled rate constants. The amplitude of the long-time fluorescence tail of ROH^* depends on the intrinsic rate constants, k_a and k_{PT} , on the proton-diffusion constant, D_{H^+} , and on the electrical potential between RO^* and the proton.

In the ESPT model described above, it is assumed that the proton is transferred to a nearby water molecule and forms an $\text{RO}^* \cdots \text{H}_3\text{O}^+$ ion pair that subsequently dissociates by proton transfer to another water molecule next to the H_3O^+ . Proton hopping within the water-hydrogen-bonded network is well-known. The mobility of a proton in water is 7 times that of sodium ion and other monovalent alkali ions. The ESPT dissociation scheme was suggested by Eigen²⁴ and Weller,²⁵ not only for the proton photoinduced transfer reaction but also as a general scheme for molecular fragmentation that forms two counterions. The important outcome of the dissociation scheme is that the concentration of the intermediate-state product, $\text{RO}^* \cdots \text{H}_3\text{O}^+$, depends on four reaction rates. The ion-pair UV-vis spectroscopic fingerprint is similar to that of RO^- ; its concentration is low, and therefore, it is difficult to identify it unequivocally. In the past, we have studied in detail by ultrafast pump-probe spectroscopy, the ESPT process of a commonly used photoacid, 8-hydroxypyrene-1,3,6-trisulfonate (HPTS or pyramine).^{26,27} The overall ESPT-to- H_2O rate constant of HPTS is $k_{PT} \sim 10^{10} \text{ s}^{-1}$. The pump-probe signal of HPTS shows a transient absorption at 520–560 nm that has a biphasic decay with a short time component of about 3 ps.^{26,27} We attributed this time component to the formation and geminate recombination of the $\text{RO}^* \cdots \text{H}_3\text{O}^+$ ion pair. This interpretation was challenged by a systematic pump-probe study by Fayer and co-workers,^{8,9} of several pyrene-based molecules, some of which lack the hydroxyl group. They concluded that, for the neutral photoacids, the dynamics are multiexponential because major charge redistribution that takes as long as 3 ps, precedes proton transfer, and this is followed by additional charge redistribution that accompanies proton transfer. Iftimie et al. recently studied²⁸ the dissociation of an acid by utilizing a long (~ 550 ps) ab initio molecular dynamics simulation. They determined the existence of three well-separated reaction time scales: $\tau_1 \sim 150$ fs, $\tau_2 = 3-5$ ps, and $\tau_3 = 25-50$ ps. The two longer time scales are consistent with a mechanism whereby the bond-breaking/bond-forming processes that accompany acid dissociation take place in two elementary steps. The second time component they attribute to an intermediate that lives for 3–5 ps.

In the current study we continued our previous effort to look for and spectroscopically identify the ion-pair intermediate $\text{RO}^* \cdots \text{H}_3\text{O}^+$. For this purpose, we measured the ESPT process of quinone cyanine-9 dye (QCy9) by several time-resolved methods as well as by steady-state UV-vis spectroscopy in both H_2O and D_2O . We found that both fluorescence and pump-probe spectroscopy show the existence of an intermediate product in the proton dissociation of QCy9. We attribute this intermediate to the $\text{RO}^* \cdots \text{H}_3\text{O}^+$ ion pair. The formation time of this intermediate is about 100 fs in H_2O and 200 fs in D_2O . The dissociation of this intermediate takes about 1 ps in H_2O and 1.6 ps in D_2O .

EXPERIMENTAL SECTION

The fluorescence up-conversion technique was employed in this study to measure the time-resolved emission of QCy9 and QCy7 in several protic solvents at room temperature. The laser used for the fluorescence up-conversion was a cavity-dumped Ti:sapphire femtosecond laser (Mira, Coherent), which provides short, 150 fs, pulses at about 800 nm. The cavity dumper operated with a relatively low repetition rate of 800 kHz. The up-conversion system (FOG-100, CDP, Russia) operated at 800 kHz. The samples were excited by pulses of ~ 8 mW on average at the SHG frequency. The time response of the up-conversion system is evaluated by measuring the relatively strong Raman-Stokes line of water shifted by 3600 cm^{-1} . It was found that the full width at half-maximum (fwhm) of the signal is 340 fs. Samples were placed in a rotating optical cell to avoid degradation. We found that, during our 5 min time-resolved measurements in a cell rotating at a frequency of 10 Hz, the degradation of the sample was marginal and had no effect on the decay profile of the signal. The QCy7 and QCy9 samples were excited in their protonated ROH form (Scheme 1). Experiments were carried out on samples at concentrations of about 1 mM or less. Ice samples were prepared by first placing the cryogenic sample cell for about 20 min at a supercooled liquid temperature of about 260 K. The second step involved a relatively rapid cooling (5 min) to a temperature of about 240 K. Subsequently, the sample froze within a few minutes. To ensure ice equilibration prior to the time-resolved measurements, the sample temperature was kept for another 10 min at about 240 K. To prevent the exclusion of the guest molecules from the bulk ice, we dope the ice with a fraction of a percent (mole ratio) of methanol. The proton diffusion constant, D_{H^+} , in methanol-doped ice, inversely depends on the methanol concentration. The smaller the methanol concentration, the larger D_{H^+} .

In this study multichannel transient-absorption pump-probe techniques were also used. The measurements were conducted

with the use of a pump–probe system (Helios, Ultrafast Systems) in a 2 mm long cuvette, and the data were analyzed with the use of commercial software (Surface Xplorer, Ultrafast Systems). The samples were pumped at a frequency of 500 Hz with 80 fs pulses generated by an optical parametric amplifier (TOPAS, Light Conversion) tuned to 415 nm. To avoid degradation, the samples were continuously stirred inside the cuvette. The temporal chirp of the white-light-continuum probe was measured in D₂O under identical experimental conditions and the data were corrected for temporal chirp with the use of a built-in algorithm.

RESULTS

Steady-State Emission. Figure 1 shows the excitation spectrum (emission measured at 690 nm) and the steady-state

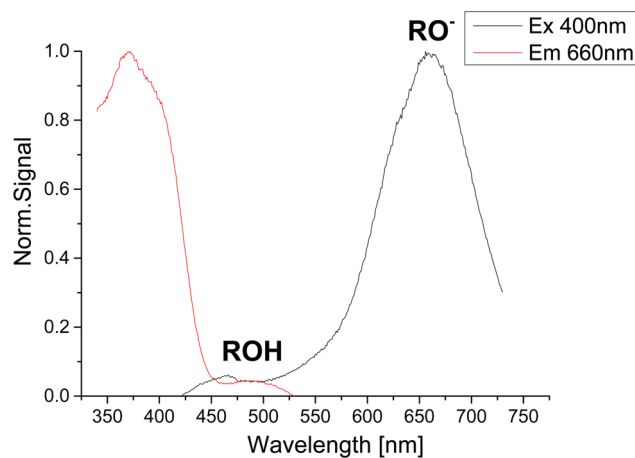


Figure 1. Excitation spectrum (emission measured at 690 nm) and the steady-state emission spectrum of QCy9 in slightly acidified aqueous solution and excited at 400 nm.

emission spectrum of the QCy9 compound shown in Scheme 1, excited at 400 nm in slightly acidified H₂O. The emission spectrum consists of two emission bands; the short-wavelength band is rather weak, with a peak at about 480 nm, whereas the intensity of the second emission band is high with a peak at about 680 nm. The short-wavelength emission band is attributed to the protonated form (ROH), and the long-wavelength band to the RO⁻ form of QCy9. The difference in the intensities of the two bands arises from several factors. The sample is excited from the

ground state in its ROH form. QCy9 is a photoacid and, as such, undergoes a photoprotolytic reaction to form the excited RO⁻ form and a proton is transferred to the water.

Steady-State Emission at Low Temperatures. Parts a and b of Figure 2 show the normalized time-integrated (steady-state) emission spectra of QCy9 in H₂O ice, over a wide range of temperatures: 80–250 K. Parts a and b of Figure 3 show the normalized time-integrated (steady-state) emission spectra of QCy9 in D₂O ice, over a wide range of temperatures, 80–240 K.

To prevent the “guest” molecule (QCy9) from being expelled from the bulk of the ice during freezing of the sample, we added to the liquid water a small amount of 0.5% mol methanol as a cosolvent. In previous studies of methanol-doped ice with organic photoacids as salts like naphthol sulfonates, we found that low concentrations of methanol prevent the aggregation of the photoacid molecule on the microcrystalline surface of the ice upon freezing of the sample.^{29–31} At high-temperature ice ($T \geq 185$ K), the emission spectrum of QCy9 in ice is similar to that in water. The spectrum consists of a weak band with a peak at ~ 500 nm assigned to the protonated form, ROH, and a strong band with a peak at ~ 670 nm attributed to the deprotonated form, RO⁻. At high temperatures ($T \geq 200$ K), the band shape and position of the RO⁻ form is almost temperature-independent for both H₂O and D₂O samples.

At lower temperatures, the spectral shape depends strongly on temperature for both H₂O and D₂O samples. The RO⁻ emission band shifts to the blue as the temperature is lowered. At $T \leq 150$ K an abrupt change is noticed in the emission spectrum; the RO^{-*} band shifts by about 1000 cm⁻¹ to the blue. Over the temperature range 115–150 K, the RO⁻ band peak position in both H₂O and D₂O is fixed at about 620 nm. We suggest that this unexpected emission band could be assigned to the ion-pair RO^{-*}...H₃O⁺, the intermediate formed following the ESPT process. We deal further with this issue in the Discussion. In D₂O samples at temperatures $T \geq 148$ K the ROD/RO⁻ band intensity ratio $I_{\text{ROD}}/I_{\text{RO}^-}$ strongly depends on the temperature, whereas in H₂O samples this equivalent ratio is much less dependent on the temperature. This difference in the temperature dependence of the spectrum of QCy9 in H₂O and D₂O is explained as follows: The ESPT rate in H₂O even at such low temperatures is larger than the radiative rate of the ROH, whereas in D₂O the rate is comparable to the radiative rate or smaller because of the ESPT kinetic isotope effect (KIE), which is about 2 at room temperature. Tunneling theories of proton/deuteron transfer³² predict that, at sufficiently low temperatures,

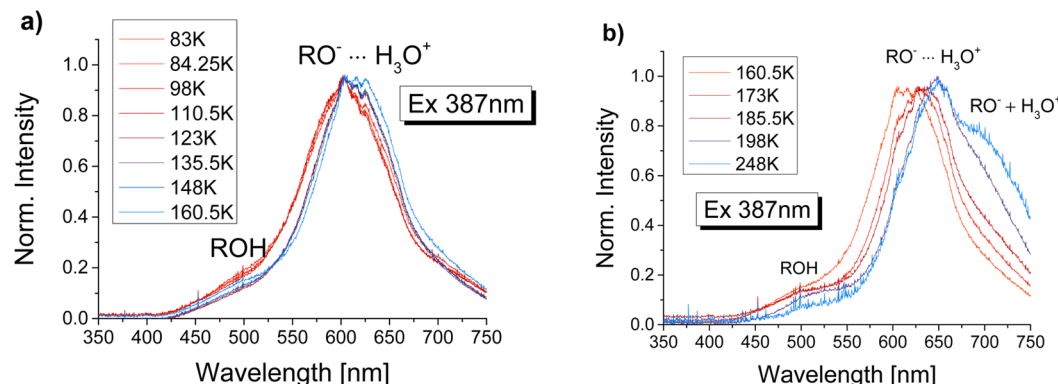


Figure 2. Normalized steady-state emission spectra of QCy9 in H₂O measured at several temperatures: (a) low (83 K) to mid (160 K) temperatures; (b) mid (160 K) to high (248 K) temperatures.

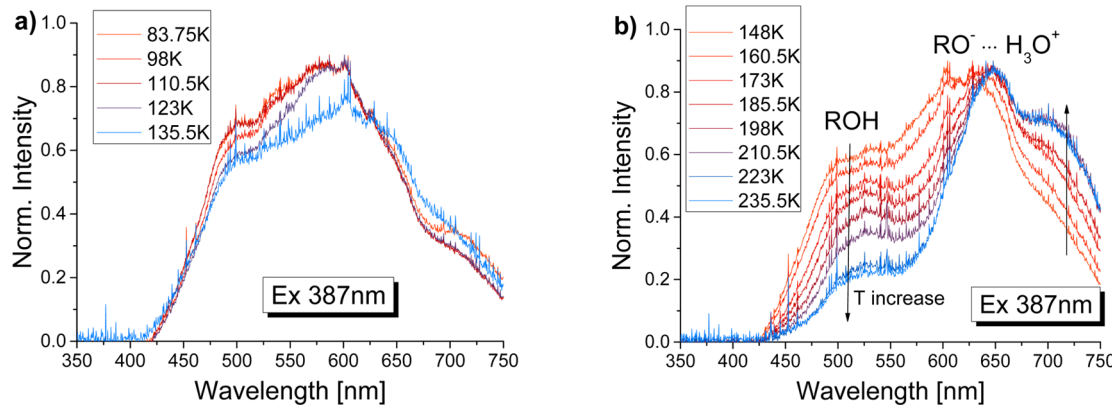


Figure 3. Normalized steady-state emission spectra of QCy9 measured at several temperatures in D_2O : (a) low (83.75 K) to mid (135.5 K) temperatures; (b) mid (148 K) to high (235.5 K) temperatures.

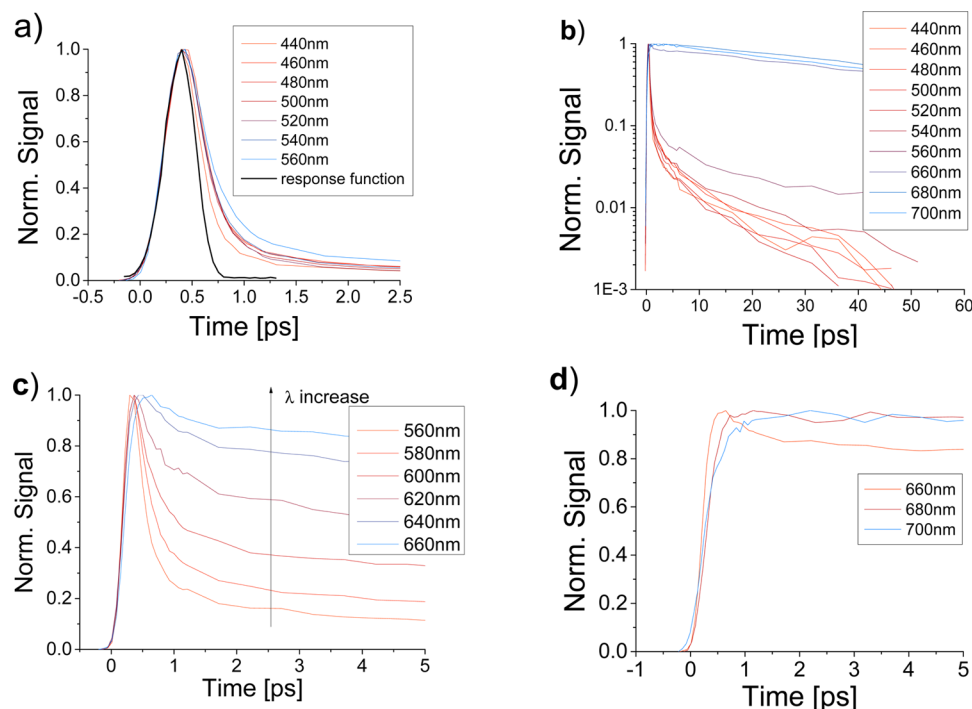


Figure 4. Fluorescence up-conversion signals of QCy9 in a slightly acidified aqueous solution: (a) linear scale, showing the upconversion response function in black; (b) normalized signal on a semilogarithmic scale with an extended time scale showing the nonexponential fluorescence tail; (c) intermediate wavelengths that show a decay component of about 2 ps, which is attributed to dissociation of the $\text{RO}^-\cdots\text{H}_3\text{O}^+$ ion pair (see text); (d) long-wavelength ($\lambda > 660$ nm) signals showing the formation of RO^* and a distant hydrated proton.

the temperature dependence of the proton-transfer rate will be smaller for H_2O than for D_2O and thus the KIE is expected to increase at low temperatures. A comparison of the experimental results shown in Figures 2 and 3 clearly shows that the temperature dependence of the $I_{\text{ROD}}/I_{\text{RO}^-}$ ratio in D_2O is much larger than in its H_2O equivalent. Further study on this subject is underway. Below 235 K, proton diffusion in neat ice decreases with temperature and the activation energy of the process is 0.2–0.3 eV, (17–28 kJ/mol), as the temperature is lowered.^{33–37} At $T \leq 150$ K, the proton is transferred from the ROH^* form of QCy9 to nearby water molecules and cannot hop any further within the excited-state lifetime of the RO^* species, which at low temperatures is ~ 3 ns. We base our interpretation on a previous study, in which a quasi-elastic neutron-scattering technique was used to measure the proton-hopping time in ice. We found that the hopping time of a proton in ice at 150 K is rather slow, about

1 ns,³⁸ whereas, at ~ 190 K it is 8 ps. We further refer to the ion-pair formation and identification in the Discussion. Similar results were previously obtained for QCy7.³⁹ QCy7 is a weaker photoacid with $\text{p}K_a^* \sim -6$ whereas QCy9 has $\text{p}K_a^* \sim -8.5$. The steady-state spectrum of QCy7 at several temperatures in both H_2O and D_2O ice is shown in Figures S1a and S1b in the Supporting Information, respectively. At low ice temperatures ($T < 165$ K) a new emission band appears and its band peak is at a wavelength intermediate between those of the ROH and RO^- bands.

Time-Resolved Fluorescence of QCy9 in Aqueous Solution with the Use of the Fluorescence Up-Conversion Technique. Parts a and b of Figure 4 show the fluorescence up-conversion signals of QCy9 in a slightly acidified aqueous solution. The sample was excited by a short (150 fs) laser pulse at ~ 385 nm at a repetition rate of 800 kHz. The

fluorescence up-conversion overall system response has a half-maximum full width of ~ 300 fs. The signals in the range 440–600 nm were fitted by a four-exponential fitting procedure. Table 1 provides the fitting parameters.

Table 1. Exponential Fitting Parameters of Up-Conversion Fluorescence of QCy9 in H₂O

λ [nm]	a_1	τ_1 [fs]	a_2	τ_2 [fs]	a_3	τ_3 [ps]	a_4	τ_4 [ps]
460	0.93	80	0.05	820	0.02	8.5	0.002	70
480	0.89	100	0.07	830	0.028	8.5	0.012	65
500	0.89	110	0.07	800	0.028	8.5	0.011	75
520	0.90	110	0.07	850	0.028	8.5	0.012	60
540	0.91	100	0.07	810	0.020	10.5	0.01	80
560	0.80	110	0.10	840	0.07	5.5	0.03	120
580	0.75	180	0.06	800	0.11	3.5	0.08	130
600	0.62	170	0.07	600	0.14	2.5	0.17	120

At short wavelengths (460–560 nm), the main decay component of the signal has an amplitude greater than 0.80 and a decay time of about 100 fs. This time component is attributed to excited-state proton transfer to the solvent. We find that the proton-transfer rate constant, k_{PT} , is $1.0 \times 10^{13} \text{ s}^{-1}$, the highest reported in the literature.¹⁹ The fluorescence signal at longer times ($t > 400$ fs), is attributed to the proton-geminate recombination to re-form the ROH* in its excited state. The repopulation process of ROH* at longer times of ~ 5 ps or more can be described by the diffusion-assisted geminate-recombination model that has been previously described.^{20,21} At these longer times, a proton-diffusion constant, D_{H^+} , can be assigned to the hopping of protons between water molecules in the bulk.

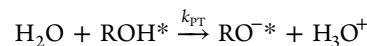
The fluorescence at long times is nonexponential because the diffusion of the proton is involved in the geminate-recombination probability. For a spherically symmetric case, the amplitude of the asymptotic long-time fluorescence tail and the time dependence of the RO⁻ form population of a reversible photoacid is given by⁴⁰

$$I_f^{\text{ROH}}(t) \sim \frac{\pi a^2 k_a \exp[-V(a)]}{2k_{\text{PT}}(\pi D t)^{d/2}} \quad (1)$$

where a is the reaction-sphere radius, k_{PT} and k_a are the intrinsic ESPT and GR rates of reactions occurring on the reaction sphere, $-V_D/a$ is the Coulomb potential between the RO⁻ and the proton in thermal-energy units ($k_B T$) at the reaction sphere ($r = a$), and d is the diffusion space dimension. This expression predicts a nonexponential fluorescence decay that fits a power law of $t^{d/2}$. The proton-diffusion constant in water is large, $\sim 9 \times 10^{-5} \text{ cm}^2/\text{s}$, and the average proton-hopping time between two

water molecules is calculated to be 1.5 ps. Between the short and long times of 0.4 and 5 ps, the fluorescence decay is also nonexponential, but in principle, a proton diffusion constant cannot be assigned for a time so short because the number of proton hops in water with an average hopping time of 1.5 ps is only 3 or less at times shorter than 5 ps after the excitation of ROH. This number of hops is too small for treating the proton motion as a diffusive process.

Figure 4c shows the fluorescence up-conversion signals of QCy9 in water in the intermediate wavelength region of 560–660 nm between the ROH and RO⁻ emission peaks. The signal consists of the ultrashort time component seen at shorter wavelengths and longer time components. As the wavelength is raised, the relative amplitudes of the ~ 100 fs time component decrease while the amplitudes of the longer time components increase. The signal expected over the intermediate spectral range for a unidirectional chemical process without an intermediate step



should lead to simple superposition of two signals

$$I(\lambda, t) = F^{\text{ROH}}(\lambda, t) + G^{\text{RO}^-}(\lambda, t) \quad (2)$$

where F^{ROH} and G^{RO^-} are the time-dependent emission spectra of the ROH and RO⁻ forms of QCy9. This simple scheme leads to exponential decay of the ROH fluorescence with a rate constant $k_{\text{PT}} + k_r$, where k_r is the radiative rate and k_{PT} is the proton-transfer rate. The RO⁻ fluorescence rises exponentially at the same rate $k_{\text{PT}} + k_r$ and then decays at a rate k'_r , the radiative rate of RO⁻.

This of course is not the real case of the time-resolved emission of a reversible photoacid. Because of the proton-geminate recombination process that repopulates the ROH*, the fluorescence decay of ROH shows a long time component (fluorescence tail). At short times $t < 5$ ps the diffusion constant is not defined (proton-hopping time $\tau = 1.5$ ps), and therefore, the diffusion assisted geminate recombination process as shown in Scheme 2 and given at eq 1 is not valid. We find that an additional time component with an average lifetime of about 2 ps exists. The amplitude of this time component is small, ~ 0.15 at 560 nm, and it further increases as the wavelength increases over the spectral range 560–640 nm. This time component may arise from an intermediate species between the reagent ROH and the product RO^{-*} + H₃O⁺. The proposed intermediate is the ion-pair RO^{-*}…(H₃O⁺)(H₂O)_n. The average lifetime of the intermediate species is about 2 ps. The average hopping time of a proton between two water molecules as deduced from the proton-diffusion coefficient in water is 1.5 ps. A large part of this

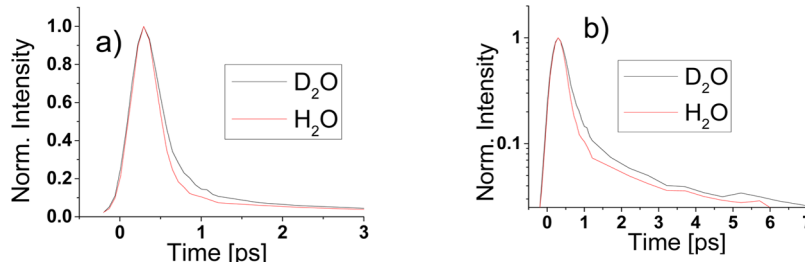


Figure 5. Time-resolved emission of the ROH/ROD form of QCy9 in H₂O and D₂O respectively, measured at 460 nm: (a) linear scale; (b) semilogarithmic scale.

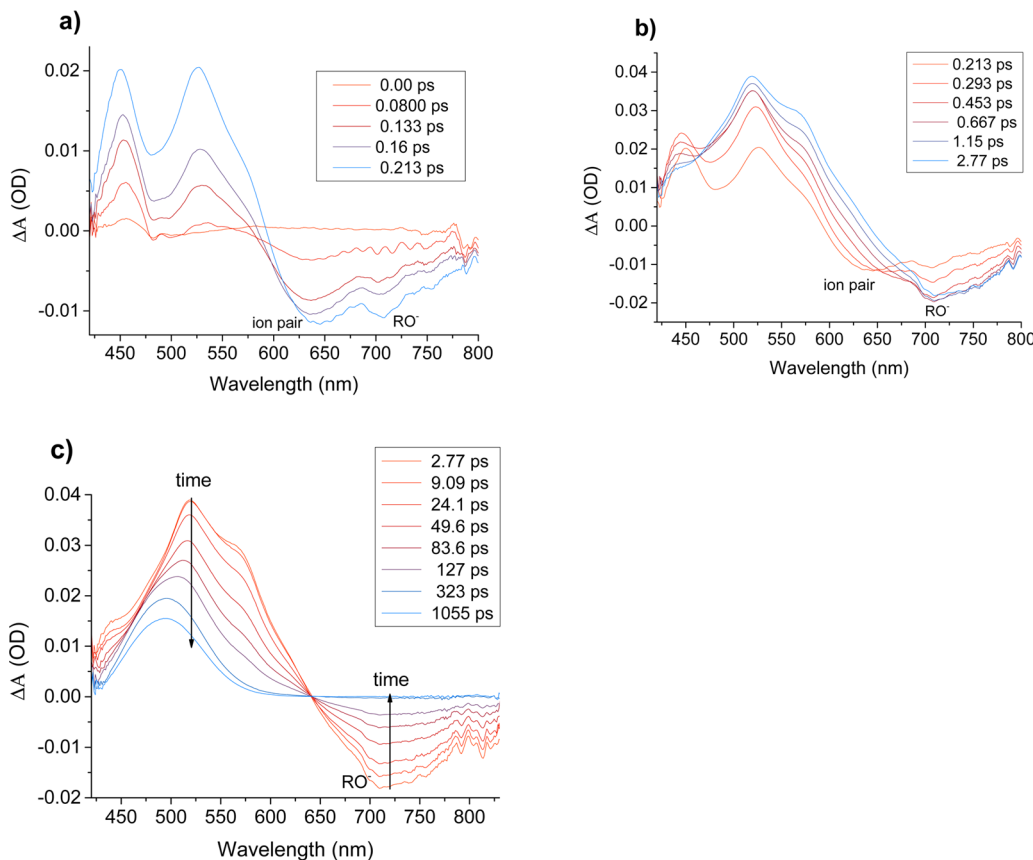


Figure 6. Time-resolved spectra of QCy9 in H₂O measured by the pump–probe optical system.

paper is devoted to the existence and characterization of the ion-pair intermediate.

Figure 4d shows the fluorescence up-conversion signal of QCy9 in water at long wavelengths (660–700 nm) that represents the RO⁻ emission band. The signal at 700 nm shows a rise longer than the instrument response function, followed by an exponential decay of about 90 ps. The rise of the signal at 700 nm is composed of at least two time components. The major component has an amplitude of 0.55 with a rise time of about 100 fs and a longer rise component with a time constant of about 1.5 ps. The longer time component is attributed to proton-hopping from the initially formed RO^{-*}··(H₃O⁺)·(H₂O)_n ion pair to a nearby water molecule, thus forming the product RO⁻ and a hydrated proton.

Figure S2 in the Supporting Information shows similar fluorescence signals for QCy9 in D₂O. The decay of the ROH signals of QCy9 in D₂O is greater than in water, and the kinetic isotope effect (KIE) is about 2. Also, the rise time of the RO⁻ signal is longer in D₂O and the fluorescence decay of RO⁻ in D₂O shows an isotope effect of about 2 and a lifetime of 180 ps as opposed to 90 ps in H₂O.

Figure 5 shows the time-resolved emission of the ROH/ROD form of QCy9 in both H₂O and D₂O respectively, measured at 460 nm. The signals clearly show the KIE of the ESPT process of QCy9 in water.

Pump–Probe Signals: Time-Resolved Pump–Probe Spectra. Figure 6 shows the time-resolved spectra of QCy9 in H₂O, and Figure S3 in the Supporting Information shows the QCy9 signals in D₂O measured by the pump–probe optical system. The spectra were recorded in the spectral range 430–800 nm. The QCy9 ROH form was excited by 410 nm 80 fs pulses at

500 Hz. We split the figure into three frames a–c. The spectra consist of positive and negative ΔA. At the ultrashort time around the zero (time) point, a water Raman signal is seen at 485 nm. The signals seen at $\lambda < 580$ nm are the sum of positive S₁–S_n absorption of the RO⁻ form and negative contributions. The negative signal is that of the ROH form emission from the S₁ state to the ground state. The cross-section of the ROH emission is larger than that of the RO⁻ emission by about a factor of 3, as could be estimated from the time-resolved emission intensity of both the ROH and RO⁻ signals measured by the fluorescence up-conversion technique shown in Figure 4. The S₁ → S_n absorption of the RO⁻ form is stronger than the ROH emission and thus at $\lambda < 580$ nm the total signal is positive. At short times a valley is noticed at around 505 nm. We attribute this valley to the contribution of the ROH emission to the total signal. With time, the ROH form disappears as a result of the photoprotolytic process described by Scheme 2. The time constant for the proton-transfer process is ~100 fs and can be measured directly by the time-resolved emission-decay rate measured over the spectral range 460–560 nm, as shown in Figure 4. The long-wavelength pump probe spectra ($\lambda > 580$ nm) consists of a negative signal that we attribute to the emission of the RO⁻ form of QCy9. This emission can also be seen in Figures 1 and 4. The peak of the emission spectrum at short times is at about 635 nm (Figure 6b,c), a wavelength much shorter than the peak of the steady-state emission spectrum where the peak position in water is at ~690 nm. As we will show later, the peak of the emission spectrum shifts to longer wavelengths with time.

Figure 6a shows the transient spectra at short times, from zero to about 0.22 ps. Over this time window the ROH form disappears and the absorption and emission spectra of the ion-

pair $\text{RO}^{\cdot\cdot}\cdots\text{H}_3\text{O}^+$ and the free RO^- forms appear. Thus, the spectra shown over this time-window can be mainly attributed to the $S_1 \rightarrow S_n$ absorption and $S_1 \rightarrow S_0$ emission of the ROH^* , $\text{RO}^{\cdot\cdot}\cdots\text{H}_3\text{O}^+$, and $\text{RO}^{\cdot\cdot}$ forms. The absorption spectrum shows that a second band at 580 nm grows with time. Two emission bands appear during this short time period, the 630 nm band we assign to the ion pair and a weaker band with a maximum at 700 nm, which appears after a certain time lag after the appearance of the 630 nm band.

Figure 6b shows the transient spectra over the time-window 0.22–2.8 ps. The intensities of the absorption and emission bands increase and large changes in band shape occur in both. The motivation of this article is to provide a clear indication of the existence of an intermediate product of the proton-transfer-to-solvent process, i.e., the $\text{RO}^{\cdot\cdot}\cdots\text{H}_3\text{O}^+$ ion pair suggested in Scheme 2. As we will show, the ion-pair concentration decreases and the free $\text{RO}^{\cdot\cdot}$ concentration of the far-removed hydronium ion increases over the time window shown in Figure 6b.

Figure 6c shows the transient spectra over the long time window of 2.8 ps to 1 ns. The RO^- emission with a constant band position at ~ 715 nm decays with a decay time of ~ 120 ps, whereas the absorption at $\lambda < 585$ nm shows a structureless long-time absorption band with a peak at ~ 515 nm. We attribute this absorption to a triplet state of the RO^- form.

Mild Acid Effect. We used trichloroacetic (TCA) acid with $pK_a = 1.7$ as a solvent to enhance the ion-pair $\text{RO}^{\cdot\cdot}\cdots\text{H}_3\text{O}^+$ contribution to the emission spectrum of QCy9. Figure 7 shows the steady-state emission and excitation spectrum of QCy9 in neat TCA acid.

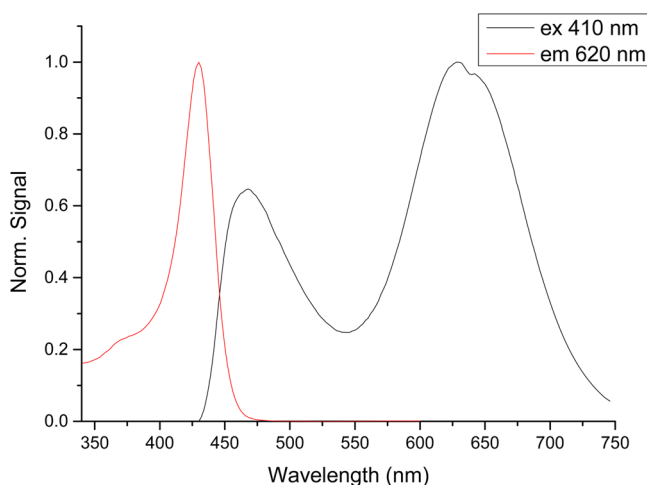


Figure 7. Normalized steady-state emission (at 620 nm) and excitation (at 410 nm) spectra of QCy9 in neat TCA acid.

In protic solvents like water and methanol the steady-state emission RO^- band consists of two sub bands, one at ~ 630 and a stronger band at ~ 670 nm (Figure 2b). In TCA acid the emission band is shifted to the blue. The band at ~ 625 nm is stronger than the sub-band at 655 nm whereas in water and alcohols the second sub-band at ~ 670 nm is stronger than the sub-band at 630 nm. We explain the inversion in the sub-band intensities by the higher $\text{RO}^{\cdot\cdot}\cdots\text{H}_3\text{O}^+$ ion-pair effective concentration of QCy9 in TCA acid. In strong mineral acid solutions the excess protons react with $\text{RO}^{\cdot\cdot}$ to re-form the ion pair and the ion pair reacts to re-form the ROH^* . In the rather weak TCA acid the reaction is somewhat different.

We assume that the proton diffusion in TCA is rather slow and the ejected proton from the ROH of QCy9 resides for a longer time in TCA than in water or alcohols on the same solvent molecule that accepted it from the ROH molecule. The geminate recombination probability is large, and therefore, the ion-pair concentration is large.

Figure 8 shows the fluorescence up-conversion signals of QCy9 in TCA acid. At 480 nm the ROH form transfers a proton to the solvent. The signal consists of fast and slow components. The fast component decay time is ~ 15 ps whereas the slow component decay is nonexponential and the average decay time $\tau_{av} \approx 200$ ps. We attribute the fast component to the ESPT process, which is rather slow in TCA, about ~ 100 times slower than in water. The TCA acid molecule is an acid with only very weak hydrogen bond accepting capabilities. The longer nonexponential tail we assign to the efficient proton geminate recombination process because of the slow proton diffusion in TCA. At ~ 600 nm close to the ion-pair emission maximum, the signal shows a distinctive rise component and subsequently a decay with a time constant of about 300 ps. We assign the rise component to the creation of the ion pair and the decay time of 300 ps is assigned to proton hopping to a distant solvent molecule. The signal measured at 660 nm shows a rather long and large amplitude rise component followed by a long exponential decay of $\tau \approx 1.5$ ns. We assign the long rise time measured at 660 nm to the formation of the RO^- from the ion pair and the long exponential decay time to the radiative decay of the RO^- of QCy9 in TCA acid. Both the steady-state and the time-resolved emission data of QCy9 in neat TCA support the current article conclusion that the photoprotolytic ion-pair intermediate spectrum could be identified in QCy9.

Figure S3 in the Supporting Information shows the time correlated single photon counting (TCSPC) time-resolved emission of QCy9 in TCA acid measured at several wavelengths in the spectral range of 460–720 nm. The TCSPC signals complement the fluorescence up-conversion signals and show with longer time resolution (instrument response time ~ 40 ps full width half-maximum) but with large dynamic range and a larger time window the emission signals of QCy9 ROH, $\text{RO}^{\cdot\cdot}\cdots\text{H}_3\text{O}^+$ and RO^- .

The TCSPC signals shown in Figure S3 (Supporting Information) measured at 560, 580, and 600 nm show an intermediate decay component with a decay time of ~ 300 ps. We assign this component to the decay of the ion pair and the generation of the free RO^- and a protonated TCA acid molecule. Figure S3c (Supporting Information) shows the exponential 1.5 ns fluorescence decay of the RO^- form. The average lifetime of the fluorescence decay signals measured by the TCSPC technique of QCy9 in TCA acid is given in Table S1 (Supporting Information).

Parts a and b of Figure 9 show the time integrated (steady-state) emission spectrum of QCy9 in several high-concentration HCl acid aqueous solutions in the concentration range of 1.4–10 M. The emission spectrum with the high-concentration 5–10 M solutions shows three emission bands, the ROH band with a maximum at 500 nm and two overlapping bands, that of the ion pair at ~ 630 nm, and the deprotonated form RO^- with a maximum at 660 nm. Band analysis using a log-normal band shape function⁴¹ reveals that at the concentration of 10 M the ion-pair emission band intensity is about 20% of the RO^- band intensity, whereas at 1.3 M the ion-pair band intensity is estimated to be about 10% of the RO^- intensity. We explain the large dependence of the ion-pair emission intensity at high acid

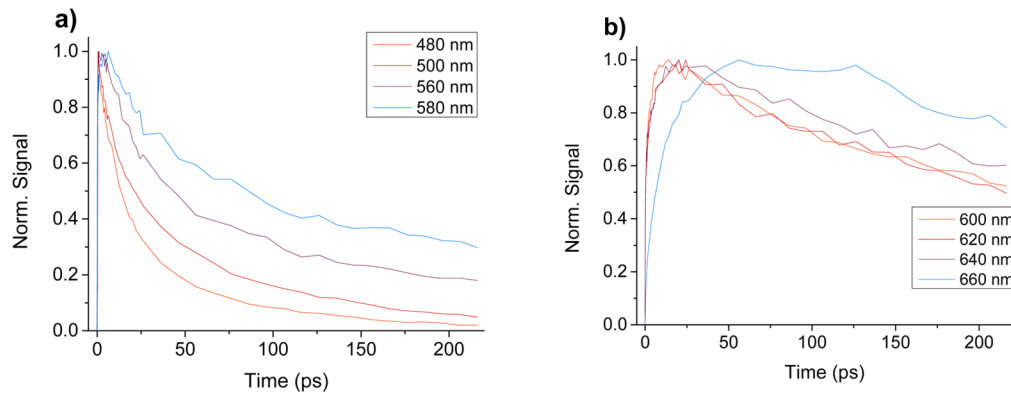


Figure 8. Normalized fluorescence up-conversion signals of QCy9 in TCA acid: (a) 480–580 nm; (b) 600–660 nm.

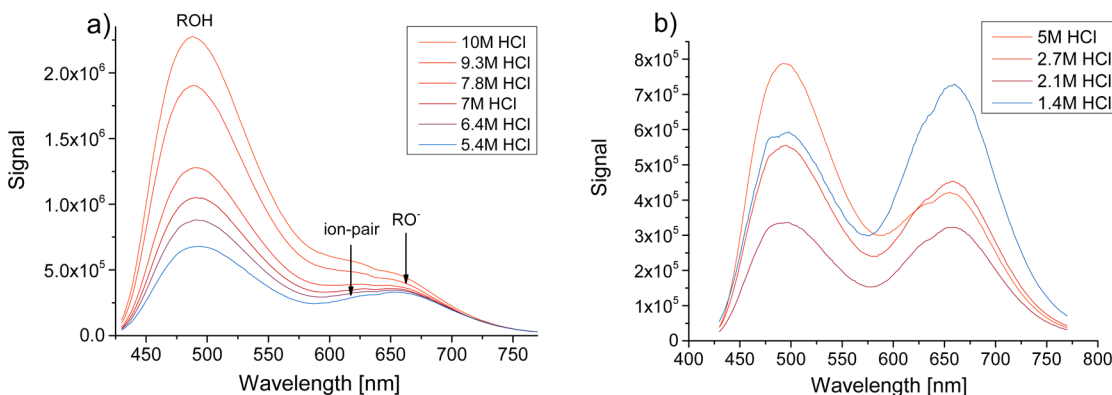


Figure 9. Time integrated (steady-state) emission spectra of QCy9 in HCl acid solutions in concentration ranges (a) 5.4–10 M and (b) 1.4–5 M.

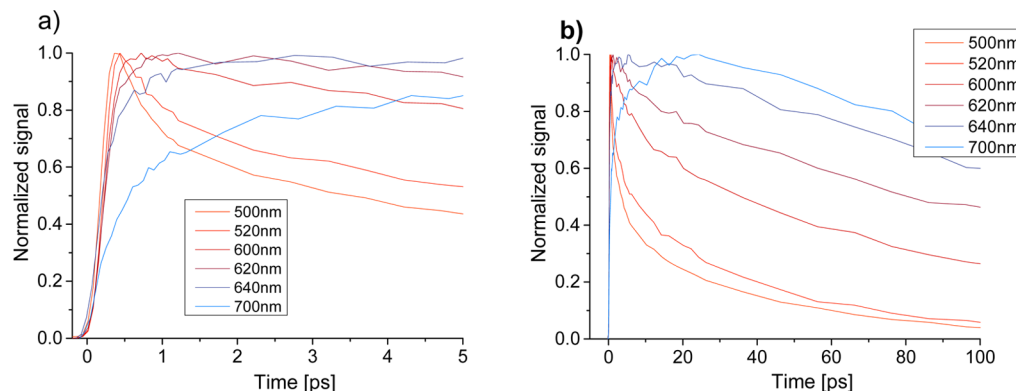
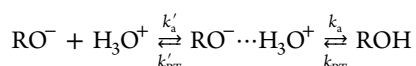


Figure 10. Fluorescence up-conversion signals of QCy9 in 5 M DCl/D₂O solution at several wavelengths: (a) at short times up to 5 ps; (b) up to 100 ps.

concentration by the large recombination rate by the reprotonation reaction of the RO⁻ form at high acid concentration.



where k'_a and k_a are the proton association rate constants of RO⁻ with excess protons in solution and the reprotonation rate to form the ROH from the ion pair, respectively. As we will show by time-resolved measurements of QCy9 in strong acids and high acid concentration, both the ion-pair time-dependent concentration and lifetime depends on the acid concentration. The larger the acid concentration the larger is the time integrated effective concentration and hence the larger intensity of the ion-pair emission band at 630 nm.

Parts a and b of Figure 10 show the fluorescence up-conversion signals of QCy9 in 5 M DCl/D₂O solution at several wavelengths. At 500 and 520 nm the ROH band maximum emission signals decay is biphasic with a short decay component of 550 fs followed by a 4.7 ps time component and a much longer decay component of 54 ps. We attribute the short decay time of 550 fs to the ESPT process to form the ion pair and the proton recombination to re-form the ROH from the ion pair occurs at ~4.7 ps. The 700 nm emission signal main contribution is that of the RO⁻ form and to a lesser extent the contribution of the ion pair. The signal rise consists of three time constants 330 fs, 3 ps, and 25 ps. The long time component we attribute to the effective decay of the ion pair to form the RO⁻ and a hydronium ion removed by at least one water molecule. This long rise time indicates that this process is about 10 times slower in 5 M HCl

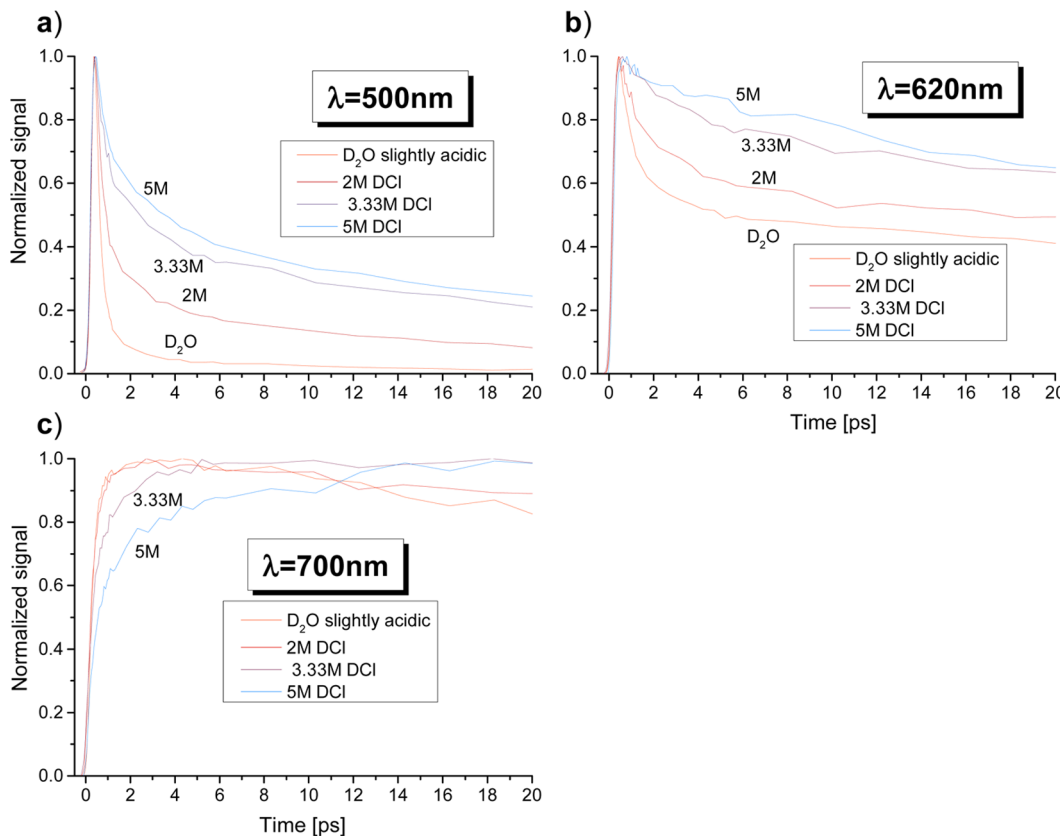


Figure 11. Fluorescence up-conversion time-resolved emission of the ROD form of QCy9 measured at 500 nm in several D_2O acidic solutions.

solution than in low acid concentrations. The large change in the reaction rate is explained by the fact that in 5 M HCl solution the fraction of free water molecules to react with the ROH or the ion pair is rather small. The strong dependence on the acid concentration of the four kinetic rate constants involved in the photoprotolytic cycle at $C_{\text{H}^+} > 1 \text{ M}$ is explained by the small effective free water concentration in such solutions. The Eigen hydrated proton H_9O_4^+ invokes four water molecules in the first solvation shell, but more water molecules are involved forming the second hydration shell. On the basis of dielectric constant measurements, Hasted et al.⁴² found that the hydration number is 10. If the hydration number is 10, then for 5 M HCl solution all the water molecules are involved in proton hydration. If that is so, then the proton-transfer rate from a photoacid to a solvent in 5 M HCl should be strongly modified. As we find in the current study, the value of k_{PT} is slowed by a factor of 3 and that of k'_{PT} forming the free H_3O^+ and separated RO^- is slower by about a factor of 8.

In a previous study³³ we measured the effect of salt concentration in aqueous solutions on the ESPT rate of 8-hydroxypyrenetrisulfonate (HPTS). For MgCl_2 and LiClO_4 we found that the ESPT decreases exponentially with salt concentration. The average hydration number of Mg^{2+} and Li^+ ions is rather large, $n \geq 7$. In 2 M of MgCl_2 or 3 M of LiClO_4 , the ESPT rate decreased by more than 1 order of magnitude. We find similar acid concentration effects on the two ESPT rate constants of QCy9.

When strong acid is added to the aqueous solution, the product RO^- reacts with the excess protons in the solution and re-forms first the ion pair that subsequently produces the ROH form. The excited-state quasi-equilibrium (shown in Scheme 2) determines the kinetics and the transient concentrations of the reactant, intermediate, and product of the photoprotolytic cycle.

The two pseudo-first-order kinetic rate constants of the two back-reactions depend on the acid concentration. At $C_{\text{H}^+} \geq 1 \text{ M}$ the back-reaction increases both the ion-pair transient concentration and the time it takes for the ion pair to disappear.

The large acid concentration modifies the four rate constants of the photoprotolytic cycle displayed in Scheme 2. The larger the acid concentration the smaller the rate constants and thus the two forward reaction rates of the proton transfer are smaller.

As for the proton recombination reaction rates, the pseudo-first-order reaction rate $k'_a C_{\text{H}^+}$ increases as the acid concentration increases but not k'_a , which decreases as the acid concentration increases.

Figure 11a shows the fluorescence up-conversion time-resolved emission of the ROD form of QCy9 measured at 500 nm in several D_2O acidic solutions using DCl as the acid. As seen in the figure, the fluorescence decay rate strongly depends on the acid concentrations. There are three time constants involved in the fluorescence decay. The short one is attributed to the PT to the solvent and the creation of the ion-pair $\text{RO}^- \cdots \text{D}_3\text{O}^+$. In neat D_2O the amplitude of the short time component is larger than 0.9 and the rate constant is $\sim 0.5 \times 10^{13} \text{ s}^{-1}$ and the decay time is $\sim 200 \text{ fs}$. In 5 M DCl the fast component amplitude decreases to ~ 0.5 and the decay time is about 600 fs, 3 times longer than in neat D_2O solution. The second decay time in neat D_2O with an amplitude of ~ 0.05 is about 1 ps and is attributed to the recombination of the ion pair to re-form the ROD. The third time component is rather long (tens of picoseconds) and is nonexponential. The long-time fluorescence tail is attributed to the geminate recombination of the proton with the RO^- after being first transferred from the ion pair to the solvent bulk. This recombination process is assisted by proton diffusion and therefore is nonexponential.^{20,21} As the acid concentration

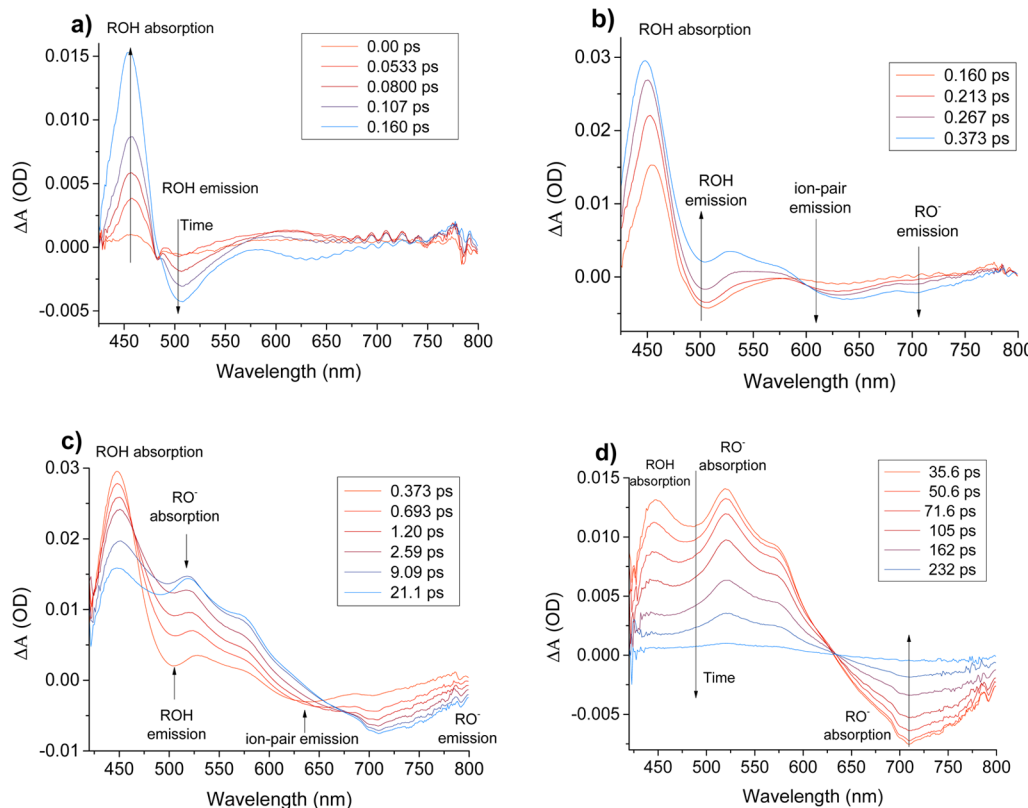


Figure 12. Time-resolved spectra of QCy9 in 6 M HCl measured by the pump–probe optical system.

increases, the second and the third time component amplitudes increase because the effective recombination rate increases when the acid concentration increases. The ion-pair recombination to re-form the ROD is not strongly affected with acid concentration but the forward reaction to create the separated RO^- and D_3O^+ is slowed considerably.

Figure 11b shows the fluorescence up-conversion signal measured at 620 nm close to the ion-pair emission band maximum, which is at 630 nm. The fluorescence signal at 620 nm consists of three contributions that of the ROD, the ion pair, and the RO^- . The ROD transition dipole moment is about 10 times stronger than that of the RO^- , which has a charge-transfer character. The RO^- band maximum is at about 665 nm and only about 1000 cm^{-1} separates the ion pair and the RO^- bands.

Figure 11c shows the fluorescence up-conversion signals measured at 700 nm of QCy9 in $\text{D}_2\text{O}/\text{DCl}$ mixtures showing mostly the RO^- form. The RO^- signal shows a rise of the signal at short time and subsequently the signal decays exponentially with a lifetime that depends only weakly on the acid concentration. The rather weak dependence of the RO^- lifetime on the acid concentration indicates that the proton recombination process is mostly reversible whereas many photoacids show that the proton recombination leads to fluorescence quenching and thus the photoprotolytic cycle is considered as irreversible.

The fluorescence rise of QCy9 in 5 M DCl solution at 700 nm consists of three time components, a fast rise time of $\tau_r \sim 300 \text{ fs}$, which is attributed to the direct formation of RO^- by the ESPT process and belongs to the red tail of the ion-pair band. It also appears at 700 nm because there is a large overlap of the ion pair and that of the RO^- bands. The second rise component of 3 ps is associated with the rate of the second step in the protolytic process in which the ion-pair D_3O^+ transfers the deuteron to another D_2O molecule and forms the RO^- and a removed D_3O^+ .

The third rise component is rather long with a time component in 5 M DCl solution of 25 ps in D_2O and 20 ps in 5 M HCl/ H_2O solution. The strong dependence of the long rise component on the acid concentration is seen in the figure. We attribute this long-time rise to the formation of the RO^- from the proton transfer of the ion-pair D_3O^+ to a nearby D_2O molecule. Although it is about 8 times longer than the intermediate rise component, we attribute both time components to the same process. We explain this rather peculiar phenomenon by the small availability of free water molecules in large acid concentrations.

Figure 12a–d shows the transient pump–probe spectra of QCy9 in aqueous solutions of 6 M HCl at several times. According to the photoprotolytic cycle shown in Scheme 2 the back-reaction rates of proton recombination should increase in acidic solutions and, therefore, the time-dependent populations of ROH^* and $\text{RO}^- \cdots \text{H}_3\text{O}^+$ should increase considerably.

Figure 12a shows the short times up to 0.160 ps. The spectrum at this short time range consists of a large absorption with a rather small bandwidth and a band peak at $\sim 463 \text{ nm}$ and an emission band with a maximum at 510 nm and also a weak broad absorption band at long wavelengths with a peak at 620 nm. An isosbestic point at $\sim 485 \text{ nm}$ and zero height is observed at these short times. We assign the strong absorption and emission bands to the ROH form of QCy9 $S_1 \rightarrow S_n$ absorption and the $S_1 \rightarrow S_0$ emission.

When comparing the transient pump–probe results of QCy9 in only slightly acidic solution at $\text{pH} \sim 5.4$, shown in Figure 6, we notice that the transient absorption at $\lambda > 480 \text{ nm}$ in Figure 6 even at early times $t < 0.2 \text{ ps}$ is missing at Figure 12. This transient absorption is assigned to the RO^- , which is seen in acidic solution only at much later times $t > 3 \text{ ps}$. At the intermediate times 0.267–0.85 ps the ROH emission decays and

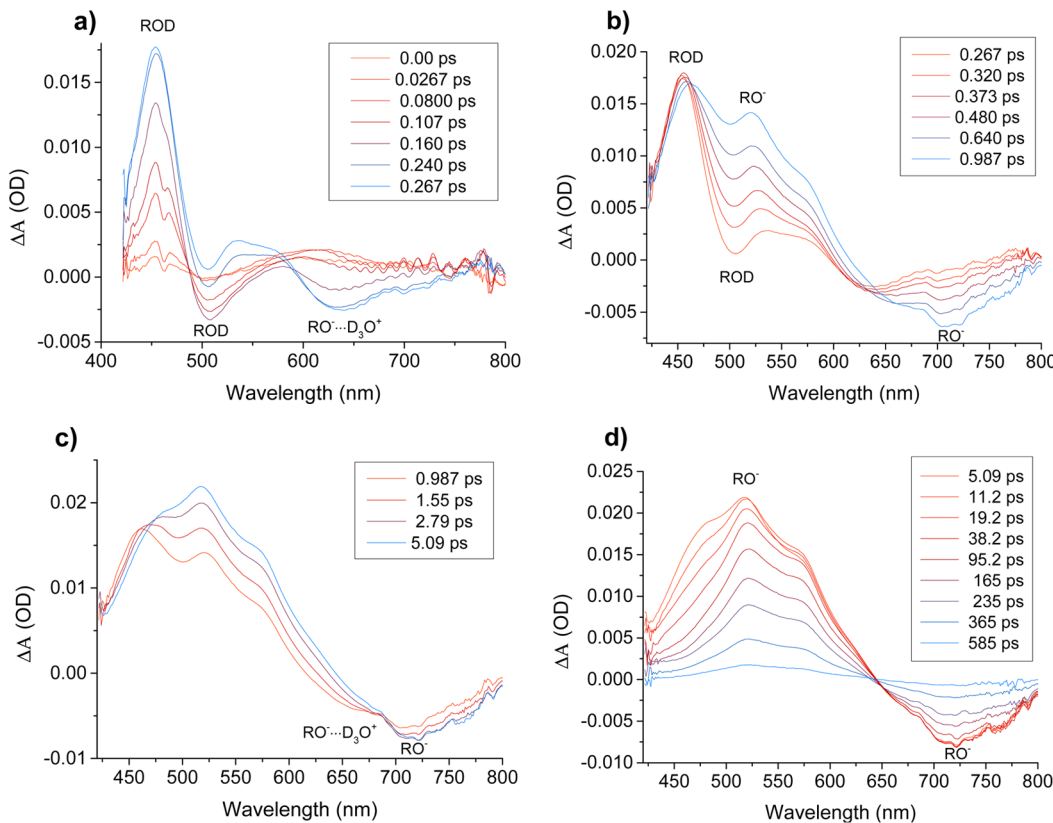


Figure 13. Time-resolved spectra of QCy9 in 3.3 M DCl measured by the pump–probe optical system.

a new broad emission band with a maximum at 630 nm grows in. We assign the new broad emission band to two new species, the $\text{RO}^-\cdots\text{H}_3\text{O}^+$ ion pair with an emission peak at 630 nm and at longer wavelengths with a band peak at 700 nm to the RO^- deprotonated form and a hydronium ion removed from the RO^- by at least one water molecule. An isoemissive point at about 580 nm separates the ROH^* emission and the $\text{RO}^-\cdots\text{H}_3\text{O}^+$ ion-pair emission.

Figure 12c shows the transient spectra at longer times from 0.9 ps to about 90 ps. The transient spectra in this time window consist of absorption and emission bands with a large overlap in the spectral range of 475–650 nm. The ion-pair emission band intensity at 630 nm decreases and a new absorption band with two maxima at 530 nm and 580 nm is clearly seen. This new band is assigned to $\text{RO}^-\text{S}_1 \rightarrow \text{S}_n$ absorption. The RO^- emission band with a band peak at 700 nm further grows in within this long time window of 90 ps.

Figure 12d shows the transient spectra at long times from ~90 ps to about 456 ps. On this time window both the positive signals and negative signals decay to zero.

Figure 13a–d shows the transient pump–probe spectra of QCy9 in an aqueous acid solution of 3.3 M DCl.

Figure S5a–d (Supporting Information) shows the transient pump–probe spectra of QCy9 in 7.5 M HCl solutions. As seen in both figures, the transient signals are similar to the transient pump–probe spectra of 6 M HCl solution shown in Figure 12. The decay time of the ROH band to form the ion pair and the RO^- emission band occur on a shorter time scale as the acid concentration decreases (when Figures 12b and 13b are compared). The RO^- emission band intensity and the RO^- maximum transient absorbance occurs on a shorter time when the acid concentration decreases. The comparison of the

transient pump probe spectra of QCy9 in strong acid results of 6, 7.5, and 10 M HCl solutions with that of slightly acidic aqueous solution of $\text{pH} \approx 5.4$ shows that the RO^- emission band reaches its maximum intensity after ~2.8 ps in an aqueous solution of $\text{pH} \approx 5.4$ whereas in an acidic solution of 6 M HCl it takes 35 ps, about 12 times longer. We attribute this striking difference to the two-step proton dissociation mechanism in which the proton can be stored at the intermediate step, i.e., the ion pair form when the excess proton concentration in the solution is large.

At 6 M HCl aqueous solution the ESPT rate of QCy9 is about 3 times slower than in neat water. The ion-pair emission band is clearly seen and decays with approximately the same time constant to form the RO^- band at 630 nm.

Main Findings.

1. Steady-state emission spectra of QCy7 (data shown in the Supporting Information) and QCy9 photoacids with pK_{a}^* of -6.5 and -8.5 in low-temperature H_2O ice ($T < 165$ K) show an abrupt and large blue band shift of the RO^- band.
2. The RO^- emission band peak at room temperature is at about 690 nm for both photoacids, whereas at $T < 165$ K the band position is at 630 nm. At temperatures of ~ 165 K, both RO^- emission bands at 630 and 690 nm coexist (Figure 2).
3. These results (1 and 2) are also valid for D_2O samples.
4. Transient pump–probe spectra of QCy9 in both H_2O and D_2O show that two absorption and two emission bands exist for the RO^- form of the photoacid at short times ($t < 4$ ps). At about 0.4 ps the main emission of the RO^- band is at a shorter wavelength (630 nm), whereas at $t > 4$ ps the dominant emission band is at 715 nm.

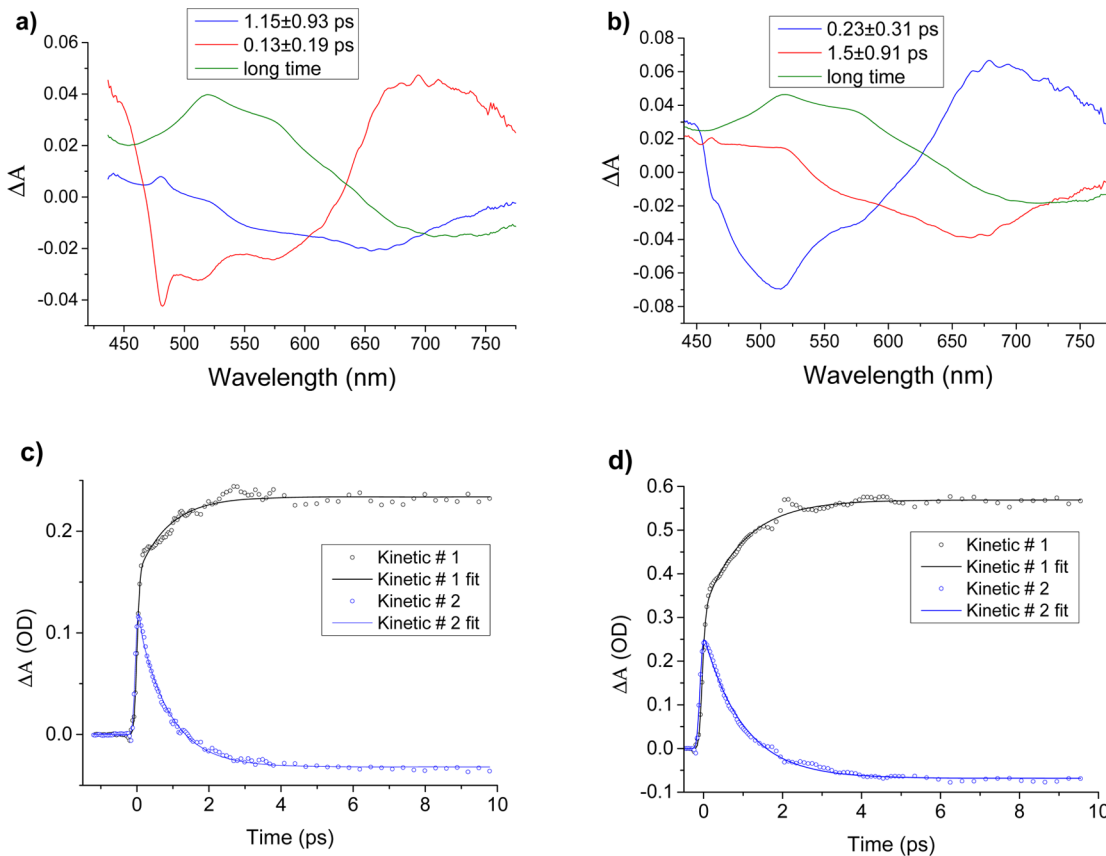


Figure 14. Global-fitting spectra derived from the analysis of the transient spectra: (a) in H_2O and (b) in D_2O and kinetic traces of the global analysis; (c) H_2O ; (d) D_2O .

5. The two transient absorption bands of QCy9 are located at 515 and 585 nm. The 585 nm band grows with a time constant of about 1 ps in H_2O .
6. We explain the findings above (1–5) by the existence at short times $t < 5 \text{ ps}$ of a contact ion-pair $RO^{-*} \cdots H_3O^+$ as an intermediate in the photoprotolytic process (Scheme 2).

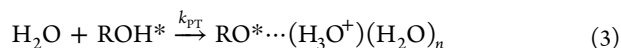
■ DISCUSSION

Global-Fitting Analysis. We used the global-fitting procedure to deconvolute the complex transient pump–probe spectra of QCy9 in water and D_2O . The data are shown in Figure 6 for H_2O and Figure S4 in the Supporting Information for D_2O ; from this procedure we obtain the relevant absorption and emission spectra of the chemical species associated with the photoacid photoprotolytic processes of proton dissociation and geminate recombination, as portrayed in Scheme 2. In short, we used singular-value decomposition,⁴³ imposing three components. The kinetic traces of these components (Figure 14c,d) were used for globally fitting the transient spectra to a multiexponential decay. Parts a and b of Figure 14 show the pre-exponential spectra derived from the global fitting analysis of the transient spectra shown in Figure 6 and Figure S4 Supporting Information).

Addition of a large amount of HCl to water modifies dramatically the water structure. Cations are known to be solvated by water molecules. The average solvation number of Na^+ is four water molecules. On the basis of the reduction of the static dielectric constant of water in the presence of ions and also excess protons, it was estimated that the average number of water

molecules that solvate a proton is 10 water molecules. At 10 M of HCl basically all water molecules are shared by the solvation of the protons and chloride ions. This strongly affects the ESPT rate of QCy9. The effective proton-transfer rate constant is reduced from about 10^{13} s^{-1} to a few tens of picoseconds, and the formation time of RO^- is about 25 ps in 10 M HCl solution.

Basically, we find three time components in the ESPT kinetics of QCy9. The first is an ultrafast time component of about 130 fs in H_2O and one of 230 fs in D_2O . These decay times correspond to the ESPT decay times of QCy9 in H_2O and D_2O , the strongest photoacid studied so far by time-resolved techniques. These decay times are somewhat longer than the decay times derived from the fluorescence up-conversion measurements of QCy9 shown in Figures 4 and 5. We previously found that the main time component of the fluorescence decay of the ROH form is ~ 100 and 200 fs for H_2O and D_2O samples.¹⁹ A comparison of the shape and amplitude of the spectra of each time component of the H_2O and D_2O samples shows that they are quite similar in both solvents. We now explain in detail the spectrum of each time component and connect it to the photoprotolytic scheme (Scheme 2) we have adopted for many years. The short time spectrum consists of negative and positive spectral components. The blue part of the spectrum ($\lambda < 600 \text{ nm}$) is negative, and we assign this part to the fluorescence of the ROH form. The fast decay time arises from the first photoprotolytic process



The proton is transferred from the ROH^* form to a nearby water molecule. A candidate for the proton-accepting water molecule is the water molecule that is hydrogen-bonded to the

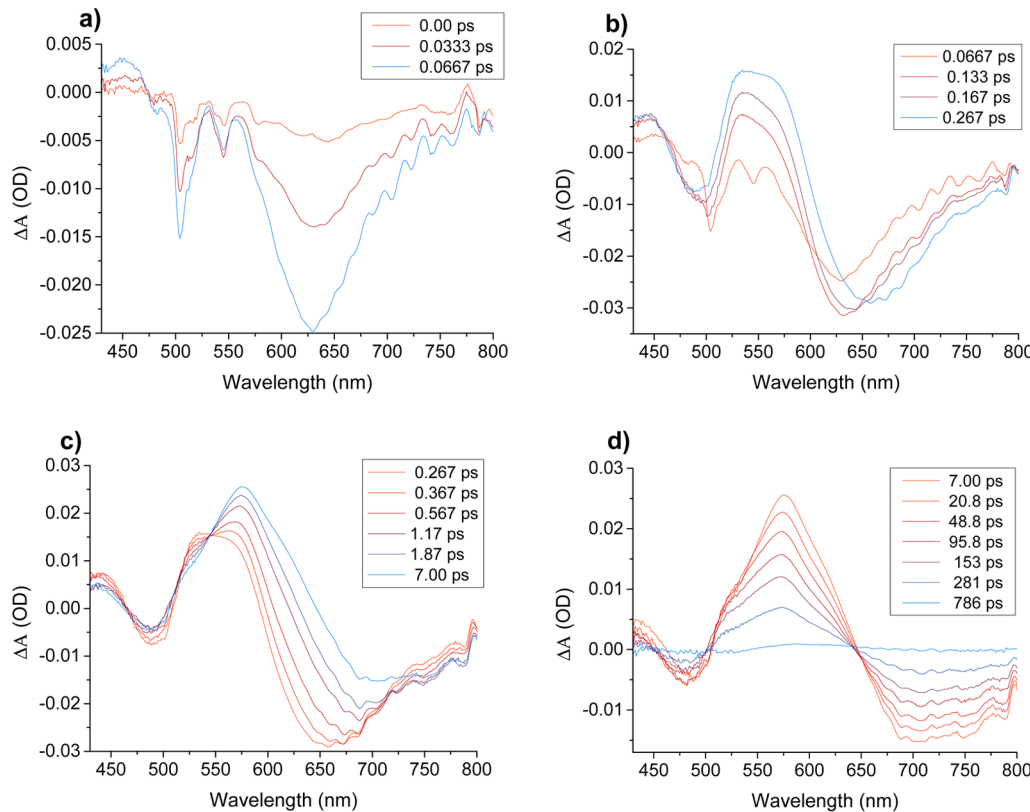


Figure 15. Time-resolved spectra of the RO^- form of QCy9 in aqueous solution at pH 8.5 measured by the pump–probe optical system.

hydroxyl group of the phenol at the center of the QCy9 molecule (Scheme 1). The ROH spectrum in H_2O (blue line in Figure 14a) shows also the water Raman–Stokes line at ~ 480 nm, shifted by about 3600 cm^{-1} from the 410 nm excitation pump pulse. The spectrum of the ROD form in D_2O shows a Raman signal at 458 nm because the OD stretch is lower in frequency (2580 cm^{-1}) than the 3600 cm^{-1} for the ROH form in H_2O . The long-wavelength absorption at $\lambda > 600$ nm arises from the transient absorption of the ROH form ($S_1^{\text{ROH}} \rightarrow S_n^{\text{ROH}}$).

The second spectrum (shown by a green line) we attribute mainly to the intermediate state, $\text{RO}^{*-}\cdots\text{H}_3\text{O}^+$, of the dissociation–association scheme (Scheme 2) of the photo-protolytic processes. The ion pair dissociates to form RO^{*-} and a hydrated proton removed at least one water molecule from the RO^{*-} . The time constants for this process as determined by the global-fitting procedure are 1.15 and 1.6 ps for H_2O and D_2O , respectively, and the kinetic-isotope-effect ratio is about 1.4 . The kinetic isotope effect of the proton/deuteron diffusion coefficient in aqueous solution, as determined by electrochemical means, is about 1.45 . Thus, this ratio of the global-fitting time constants is expected if proton or deuteron hopping between adjacent water molecules is involved in this time component. The average hopping time of a proton (or deuteron) in water as derived from the proton-diffusion coefficient is 1.5 ps, which is close enough to the global-fitting time constant of the intermediate spectrum. The intermediate global-fitting spectrum shows emission bands at 540 and 640 nm for both H_2O and D_2O samples. The amplitude of the 540 nm band is rather small compared to the fluorescence up-conversion short time component measured at 540 nm that we assigned to the ROH species. This may arise from the cancellation of positive absorption ($S_1^{\text{RO}^-} \rightarrow S_n^{\text{RO}^-}$) by the negative emission signal, because the contributions of both

ROH^* and RO^{*-} interfere at this intermediate time (Scheme 2). Because the proton is located close to the phenolate in the ion-pair configuration, a fast equilibrium exists between proton-geminate recombination and the dissociation steps which lead to the two emission spectra, that of ROH^* at 540 nm and that of the $\text{RO}^{*-}\cdots\text{H}_3\text{O}^+$ ion pair at 640 nm. The dissociation of an acid was studied by ab initio molecular dynamics simulation.²⁸ They found three well-separated reaction time scales: $\tau_1 \sim 150$ fs, $\tau_2 = 3\text{--}5$ ps, and $\tau_3 = 25\text{--}50$ ps. The two longer time scales are consistent with the mechanism shown in Scheme 2 in which acid dissociation takes place in two elementary steps. The second time component they assigned to the ion-pair intermediate that lives for $3\text{--}5$ ps. In the current study we identify both the emission spectrum and the transient absorption of the ion-pair intermediate of the QCy9 photoacid.

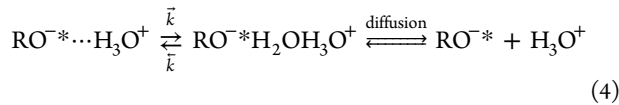
The third spectrum (shown by a red line) of the third time component of the global fit is assigned to the RO^{*-} where the transferred proton is further removed from the vicinity of the RO^- by successive proton hopping between adjacent water molecules. The spectrum decay shown by the red line is about 90 ps for water and 180 ps for D_2O . These time constants refer to the excited-state lifetimes of the RO^{*-} form of QCy9 in H_2O and D_2O , respectively. The time-resolved emission measured by the fluorescence up-conversion technique or by a time-correlated single-photon-counting technique, provide similar decay times of the RO^- in both H_2O and D_2O .

The RO^{*-} species absorbs in the blue region of the spectrum. This absorption is assigned to the $S_1^{\text{RO}^-} \rightarrow S_n^{\text{RO}^{*-}}$ transitions. The RO^{*-} emission is clearly seen in the steady-state emission spectrum shown in Figure 1. The red emission peak position is at 680 nm in aqueous solution. The long-decay-time global-fit spectrum (red) shows an emission band slightly shifted to the red

with a maximum at 700 nm. This is explained by the fact that the pump–probe signal consists of two overlapping contributions (a strong positive contribution and a weaker negative one) and the superposition of the two shifts of the emission peak to a longer wavelength. To summarize, the global fit procedure provides three time constants and three spectra that can be assigned to the three species involved in the photoprotolytic processes shown in Scheme 2. The important outcome of the global-fit procedure is that, for the first time in photoacid research, we have a good and reliable spectrum of the $\text{RO}^{\cdot\cdot\cdot}(\text{H}_3\text{O}^+)(\text{H}_2\text{O})_n$ ion pair, the intermediate of the ESPT process of a photoacid. At a sufficiently low temperature, the proton diffusion constant is small. Within the excited-state lifetime of about 0.5 ns the proton resides next to the phenolate of the QCy9 molecule and the $\text{RO}^{\cdot\cdot\cdot}\text{H}_3\text{O}^+$ ion spectrum is obtained.

In the past, we had invoked the existence of an ion pair as an intermediate step in the photoprotolytic process, but we were unable to provide direct reliable evidence for its existence at room temperature.^{26,27} The ion-pair spectrum is clearly seen at low temperatures, not only in QCy9 but also in QCy7 for a low-temperature steady-state-emission study³⁹ and also shown in Figure S1 in the Supporting Information.

The transient spectra contain the contributions of two forms of the RO^- of the QCy9–water complex. The first spectrum, which is dominant at early times, is that of a contact ion pair, $\text{RO}^{\cdot\cdot\cdot}\text{H}_3\text{O}^+$. The proton resides on a water molecule and forms a hydronium ion. In the “Zundel”-like description,^{44,45} the proton is situated between the oxygen atom of the $\text{RO}^{\cdot\cdot\cdot}$ form of QCy9 and the nearest water molecule. The water molecules surrounding this complex form hydrogen bonds with the oxygen atom of $\text{RO}^{\cdot\cdot\cdot}$ and the two hydrogen atoms of the water molecule. The transient absorption band peak assigned to the contact ion pair is at 515 nm, whereas the peak of the emission $S_1 \rightarrow S_0$ transition is at ~ 635 nm. The second form of the $\text{RO}^{\cdot\cdot\cdot}$ is a free $\text{RO}^{\cdot\cdot\cdot}$ solvated by water molecules including a hydrogen bond from a water molecule at the $\text{RO}^{\cdot\cdot\cdot}$ oxygen atom and a hydronium ion at a longer distance from the $\text{RO}^{\cdot\cdot\cdot}$ oxygen atom (see below). The kinetics of the proton transfer that chemically describes the transient spectra is given by



The $\text{RO}^{\cdot\cdot\cdot}\text{H}_3\text{O}^+$ absorption and emission spectra differ from those of $\text{RO}^{\cdot\cdot\cdot}\text{H}_2\text{OH}_3\text{O}^+$ and $\text{RO}^{\cdot\cdot\cdot} + \text{H}_3\text{O}^+$. We assume the latter forms, $\text{RO}^{\cdot\cdot\cdot}\text{H}_2\text{OH}_3\text{O}^+$ and $\text{RO}^{\cdot\cdot\cdot} + \text{H}_3\text{O}^+$, have similar spectra and thus in the analysis, we treat them as having the same spectra.

Solvation Dynamics versus Ion Pair as an Intermediate: Transient Pump–Probe of the RO^- Form of QCy9. We measured the transient pump–probe spectra of the RO^- of QCy9 in slightly basic aqueous solution pH ~ 8.5 . At this pH most of the QCy9 is in the ground-state RO^- form, because the $\text{p}K_a$ is ~ 5.5 . We excite the sample at 500 nm, near the RO^- absorption band maximum. Figure 15 shows the pump–probe transients of the RO^- of QCy9 in aqueous solution of pH 8.5.

At ultrashort times $t < 200$ fs the emission peak is at 630 nm. An absorption band assigned to the $S_1^{\text{RO}^-} \rightarrow S_n^{\text{RO}^-}$ appears at shorter wavelengths with a maximum at 550 nm that also shifts to the red with time. At times 0.4–1.8 ps the emission band shifts to the red and the $\text{RO}^{\cdot\cdot\cdot}$ band maximum reaches 690 nm and the band intensity decreases by almost a factor of 3. The absorption

band intensity increases by only 50% and also shifts to the red and the band maximum at $t = 1.0$ ps is at 575 nm. The global analysis fits nicely to two exponentials $\tau \approx 0.9$ ps and ~ 170 ps, as shown in Figure S6 in the Supporting Information.

The global analysis shown in figure S6 in the Supporting Information shows at short times a broad emission spectra at 630 nm that shifts to the red with a time constant of 0.9 ps and the transient spectrum at $t > 1$ ps consists of an absorption and emission spectrum with a maxima at 575 and 690 nm, respectively. The decay time back to the ground state is about 170 ps. The transient pump–probe spectra obtained for the RO^- excitation at 500 nm shows at long times $t > 1$ ps a pattern similar to that of the transient spectra obtained when the ground-state ROH form is excited at 400 nm. Both transient spectra show at short times an emission band at 630 nm that at longer times disappears and a band with a maximum at about 700 nm is formed.

The main evidence for advocating for an ion-pair intermediate in the photoprotolytic cycle of the ROH* form of QCy9 is given in the current manuscript as the existence of a 630 nm emission band at short times assigned to the ion pair and the disappearance at longer times of the 630 nm band and the formation of an emission band of 700 nm assigned to the $\text{RO}^{\cdot\cdot\cdot}$. We claim that the similarity of the pump–probe transient spectra at $\lambda > 600$ of ROH and RO^- excitation does not contradict our assignment of the ion-pair emission band at 630 nm. There are large enough differences in the transient spectra between the acid solution ROH excitation and the base solution RO^- spectra that provide strong evidence to the existence of an intermediate ion pair.

1. The emission band maximum intensity at 700 nm depends on the acid intensity
2. The intensity of the emission at 630 nm is 2 times weaker than that of the 700 nm when the ROH form is excited at 400 nm (Figure 6, slightly acidic, or Figures 12 and 13, acidic). The opposite occurs when the RO^- form is excited at 500 nm where the intensity at 630 nm is 2.5 times larger than the maximum intensity at 700 nm.
3. When excited at 400 nm, the band at 630 nm does not shift with time, but rather the 630 nm band intensity declines and the band intensity at 700 nm increases and a quasi isoemissive point appears at about 640 nm. When the RO^- form is excited, the emission band red shift is accompanied by a strong band intensity reduction that occurs as time progresses. This pattern is not observed when a photocycle starts with ROH excitation

Identifying a short-lived intermediate in a chemical reaction in solution is not at all trivial. The main obstacle in unequivocally determining an intermediate with similar spectral properties as the final product (as is the case in the current article) is the solvation dynamics of the initially formed (excited) intermediate or that of the final product.

The pump–probe transient spectra shown in Figures 6, 9, and 10 show an emission band with a maximum at 630 nm and an emission band with a maximum at 700 nm. The generation and decay of the emission band at 630 nm is much faster than the dynamics of the emission band with a maximum at 700 nm. Our interpretation of the transient spectral evolution is that the band with a maximum at 630 nm is the missing ion-pair intermediate given in the photoprotolytic scheme (Scheme 2). In neutral pH aqueous solution the intermediate spectra is short-lived and disappears at about 1.5 ps. This is also the expected time scale for

Table 2. Fitting Parameters of the Pump–Probe Data, Spectral Analysis

time (ps)	RO ⁻ ...H ₃ O ⁺ absorption				RO ⁻ H ₂ OH ₃ O ⁺ absorption			
	<i>h</i> ₁	<i>v</i> _{p1} (cm ⁻¹)	Δ <i>v</i> _{p1} (cm ⁻¹)	γ ₁	<i>h</i> ₂	<i>v</i> _{p2} (cm ⁻¹)	Δ <i>v</i> _{p2} (cm ⁻¹)	γ ₂
0.347	0.4	19 240	1900	0.3	0.28	17 550	1900	0.05
0.507	0.4	19 280	1900	0.3	0.31	17 550	1900	0.05
0.667	0.4	19 310	1900	0.3	0.33	17 550	1900	0.05
0.9887	0.4	19 340	1900	0.3	0.35	17 550	1900	0.05
1.55	0.4	19 360	1900	0.3	0.36	17 550	1900	0.05
3.85	0.4	19 380	1900	0.3	0.37	17 550	1900	0.05
time (ps)	RO ^{-*} + H ₃ O ⁺ emission				RO ^{-*} H ₂ OH ₃ O ⁺ emission			
	<i>h</i> ₃	<i>v</i> _{p3} (cm ⁻¹)	Δ <i>v</i> _{p3} (cm ⁻¹)	γ ₃	<i>h</i> ₄	<i>v</i> _{p4} (cm ⁻¹)	Δ <i>v</i> _{p4} (cm ⁻¹)	γ ₄
0.347	-0.32	15 500	2400	-0.05	-0.16	13 750	2400	-0.3
0.507	-0.24	15 500	2400	-0.05	-0.21	13 750	2400	-0.3
0.667	-0.21	15 500	2400	-0.05	-0.23	13 750	2400	-0.3
0.9887	-0.18	15 500	2400	-0.05	-0.245	13 750	2400	-0.3
1.55	-0.13	15 500	2400	-0.05	-0.25	13 750	2400	-0.3
3.85	-0.05	15 500	2400	-0.05	-0.26	13 750	2400	-0.3

solvation dynamics that shift an emission band to the red in aqueous solution. In acidic solutions the 630 nm band exists in the transient pump–probe spectra for a long time, more than 20 times longer than in a neutral pH solution. Figure 10c shows that it could be identified even at long times up to 50 ps. Solvation dynamics shifts the emission band to lower energies as a function of time.

The main solvent–solute interactions that are responsible for the band shift are dipolar, dispersion, and hydrogen-bond formation or breaking and also weakening or strengthening of existing solute–solvent hydrogen bonds. When a photochemical reaction takes place, A^{*} → B^{*}, and the two emission bands overlap to a large extent, it is often quite difficult to determine that such a reaction indeed occurs and many times the identification that such a reaction occurs is replaced by the competing solvation dynamics process.

For water the solvation dynamics is ultrafast with short lifetime components of less than 100 fs and the longest component decay time is about 0.75 ps. An important experimental observation is that solvation dynamics of an excited molecule are almost identical for H₂O and D₂O. We found in this study an isotope effect of ~1.5 of the decay kinetics of the intermediate emission band at 630 nm. This fact is in favor of assigning the 630 nm emission band to the RO^{-*}...H₃O⁺ ion pair.

For example the chemical structure of curcumin, shown in Scheme S2 (Supporting Information), may suggest that it undergoes several photoreactions in its excited state. The two phenols of curcumin may show photoacidic properties whereas the diketo group at the center may undergo an intramolecular proton-transfer reaction. The single broad emission band position and intensity of curcumin depends on the solvent viscosity and polarity. Palit and co-workers⁴⁶ explain the time-resolved curcumin emission results in 16 solvents as arises from solvation dynamics. Our studies^{47–49} have shown that curcumin in the excited state can act as either a photoacid in protic solvents or a photobase in acidic solvents. We found that the broad emission band of curcumin in many protic solvents could be decomposed to two emission bands, the blue part of the spectrum for the ROH^{*} band and the red part for the RO^{-*} band, or in acidic media, the ROH₂^{**} band, the protonated form of curcumin.

Pump–Probe Spectral Analysis. In this subsection, we analyze the transient pump–probe spectra of QCy9 in water over

the short time window of 0.35–3.8 ps. We notice that over this time window, shown in Figure 6b, the absorption and emission band intensities are almost constant, whereas there are large changes in the band structure. We noted that both the absorption and emission spectra could be resolved into two main bands. The two absorption bands have peaks at 515 and 585 nm. The intensity of the 585 nm band increases, while that of the 515 nm band decreases slightly with time. The emission band could also be resolved into two emission bands with peaks at 630 and 715 nm. With time, the intensity of the 630 nm band decreases, while that of the 715 nm band increases. We fit the shape and height of the spectral bands (*F*₁(λ)) for each measured time over the time range of 0.35–3.8 ps by a log-normal spectral-line-shape function (Suzuki,⁴¹ Maroncelli⁵⁰):

$$I(\nu) = h \begin{cases} \exp[-\ln(2)\{\ln(1+\alpha)/\gamma\}^2] & \alpha > -1 \\ 0 & \alpha \leq -1 \end{cases} \quad (5)$$

$$\alpha \equiv 2\gamma(\nu - \nu_p)/\Delta\nu_p \quad (6)$$

The log-normal function has four adjustable parameters (*h*, *ν*_p, Δ*ν*_p, and γ). *ν*_p is the band-peak position, *h* is the band intensity, Δ*ν*_p is the bandwidth, and γ is the asymmetry of the band. When γ = 0, the line shape is Gaussian. Table 2 provides the four fitting parameters of the two absorption and two emission bands.

For absorption bands (S₁(0) → S_n(ν=n)), the asymmetry parameter of the bands is positive, whereas for emission bands (S₁(0) → S₀(ν=n)), it is negative. The bandwidth of both absorption bands is 1900 cm⁻¹, whereas for the two emission bands, it is 2400 cm⁻¹. The emission-band asymmetry of the contact ion pair is small (γ = -0.05) but is larger for the free RO^{-*} + H₃O⁺ (γ = -0.3). This difference can be explained by the more rigid structure of the ion-pair complex compared to that of the free RO^{-*}, for which the solute–solvent interactions are more dispersed. Another important aspect of the analysis is the difference of 1750 ± 50 cm⁻¹ in energy between the two absorption bands. The same energy difference also holds for the two emission bands. The energy difference of about 0.22 eV of the RO^{-*} spectrum arises from the large Coulomb interaction of the RO^{-*}...H₃O⁺ ion-pair structure on the electronic states involved in the optical transitions shown in the transient spectra. The emission-intensity ratio *I*_{RO⁻H₃O⁺}/*I*_{RO⁻H₂OH₃O⁺} varies from 2 at 0.35 ps to about 0.2 at 3.8 ps. Thus, the concentration of the

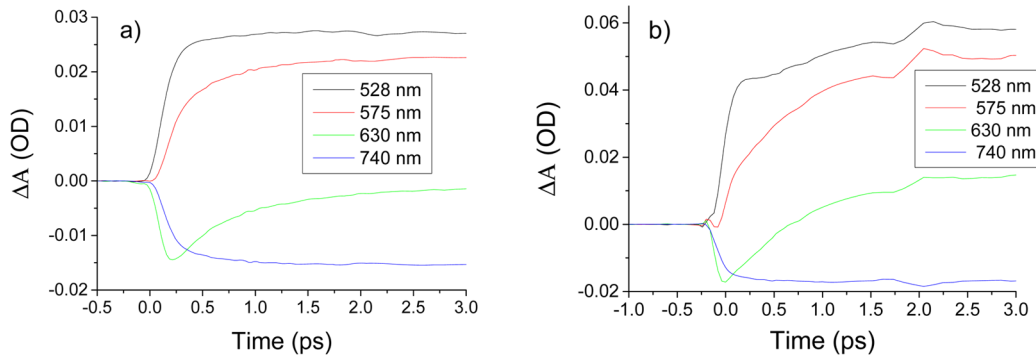


Figure 16. Pump–probe time-resolved signals of QCy9 at specific wavelengths assigned the $\text{RO}^{-\bullet}$ and $\text{RO}^{-\bullet}\cdots\text{H}_3\text{O}^+$ absorption and emission band peaks in (a) H_2O and (b) D_2O .

contact ion pair (the intermediate product of the photoprotolytic reaction) decreases within a few picoseconds by a factor of ~ 10 and most of the protons are released to bulk water.

Figure S7 in the Supporting Information shows the experimental transient pump–probe spectra over the time range 0.35–3.8 ps and their fitting by the log-normal line-shape function. The fit consists of two absorption bands, that of the intermediate product $\text{RO}^{-\bullet}\cdots\text{H}_3\text{O}^+$ and the band of the free $\text{RO}^{-\bullet}$ and hydronium ion far removed from the nearest $\text{RO}^{-\bullet}$ molecule. The fit to the experimental transient spectra is rather good at six different time points in the range 0.35–3.8 ps where the $\text{RO}^{-\bullet}\cdots\text{H}_3\text{O}^+$ spectrum converts into $\text{RO}^{-\bullet} + \text{H}_3\text{O}^+$ spectrum. These analysis results support the dissociation scheme of photoacids as portrayed in Scheme 2 and also support the global analysis shown in Figure 14.

Parts a and b of Figure 16 show the time-resolved pump–probe signals of QCy9 in H_2O and D_2O samples respectively, measured at four wavelengths (528, 575, 630, and 740 nm). At 528 nm, the $\text{RO}^{-\bullet}\cdots\text{H}_3\text{O}^+$ absorption peak, the signal intensity from about 300 fs and up to about 5 ps, is almost independent of time. In contrast to the signal intensity at 528 nm, at 575 nm the signal rise is composed of two time components, a short time component of ~ 100 fs and a longer one of ~ 1 ps. We attribute the longer rise-time component to the dissociation of the $\text{RO}^{-\bullet}\cdots\text{H}_3\text{O}^+$ ion pair to form a free $\text{RO}^{-\bullet}$ and detached H_3O^+ . The time-resolved spectrum consists of two negative components that are attributed to emission from $\text{RO}^{-\bullet}$ to the ground state. The emission at 630 nm is assigned to the $\text{RO}^{-\bullet}\cdots\text{H}_3\text{O}^+$ ion pair, and that at 740 nm to the free $\text{RO}^{-\bullet}$. The $\text{RO}^{-\bullet}\cdots\text{H}_3\text{O}^+$ emission forms at about 100 fs and decays with a time constant of about 1 ps in H_2O . The 740 nm emission exhibits a signal rise of two components, a short one with a rise time of about 100 fs and a long one of about 1 ps. The 740 nm emission is attributed to the free $\text{RO}^{-\bullet}$ form and a detached hydronium ion. In summary, the time-resolved spectra shown in Figure 6 fit the overall picture of two absorption and two emission bands, obtained from the detailed spectral analysis given above. The four bands are broad with bandwidths of 1900 and 2400 cm^{-1} for the absorption and emission bands, respectively. The space between the bands is small, only 1750 cm^{-1} . This, of course, causes a large overlap of the individual bands. The band overlap strongly affects the time-resolved emission signals, and therefore, two time components are seen.

Spectroscopic Identification of the Ion-Pair $\text{RO}^{-\bullet}\cdots\text{H}_3\text{O}^+$ at Low Temperatures. Parts a and b of Figure 2 show the steady-state emission of QCy9 in H_2O and D_2O ice, respectively. In H_2O between 83 and 160 K, the emission spectrum consists of

two emission bands, a broad band assigned to the ROH/ROD form with a peak at 560 nm and a weaker band at about 620 nm, which we assign to the ion-pair $\text{RO}^{-\bullet}\cdots\text{H}_3\text{O}^+$. This peak is blue-shifted by about $\sim 1700 \text{ cm}^{-1}$ from that of the $\text{RO}^{-\bullet}$ emission band (700 nm) at higher temperatures of $T \geq 197 \text{ K}$. Scheme 2 portrays the proposed mechanism of the photoprotolytic proton dissociation and recombination as well as the relaxation of the electronically excited photoacid and the conjugated base back to the ground state.

We propose that the proton-dissociation reaction intermediate is an ion pair consisting of the $\text{RO}^{-\bullet}$ and a hydronium ion next to the phenolate. This intermediate was suggested for acid–base dissociation and recombination reactions by Eigen more than half a century ago.²⁴ The following step involves dissociation by proton transfer between the hydronium ion formed and an adjacent water molecule. The reverse reaction leads to recombination and re-formation of the ROH^* . The population of the ion-pair transient strongly depends on the four rate constants shown in Scheme 2.

On the basis of knowledge recently acquired^{51–59} by IR studies concerning proton hydrates at high temperatures ($>227 \text{ K}$), ion pairs of $\text{RO}^{-\bullet}$, if they exist, are large hydrates with $\text{H}_{13}\text{O}_6^+$ cations developed, which produce the QCy9 emission band at 690 nm. The positive charge on this hydronium cation is significantly delocalized as a result of high proton mobility, because the distance between the negative and positive centers of charge is large. If the temperature is lowered to 160 K, the dynamic properties of the proton in H_{aq}^+ clusters are reduced, and this results in an increasing charge concentration at the center of the cluster and the production of more tightly formed ion pairs. This produces in the spectra a gradual blue-shifting of the QCy9 emission band to 680 nm. Then at $T < 150 \text{ K}$ the abrupt change in the spectrum is observed, because the ion pair is converted to a proton disolvate of $\text{L}_1-\text{H}^+-\text{L}_2$, where L_1 is the $\text{RO}^{-\bullet}$ anion and L_2 is H_2O with H^+ shared more or less equally between the two.

The intermediate state of $\text{L}_1-\text{H}^+-\text{L}_2$ type species, with a short, and therefore strong, hydrogen bond with two well or flat-bottom hydrogen potentials, is well-known. Asymmetric proton disolvates, $\text{L}_1-\text{H}^+-\text{L}_2$, are much less stable than symmetric, $\text{L}-\text{H}^+-\text{L}$, disolvates and have a narrower region of existence. Formation of anion– H^+-OH_2 intermediates for acids is known from the literature.

The hopping time of a proton in low-temperature ice was recently measured for HCl-doped ice by the quasi-elastic neutron-scattering technique (QENS).³³ It was found that the hopping time is $\sim 1 \text{ ns}$ at 150 K, whereas at 190 K it is rather short

(8 ps). The activation energy of the hopping in this temperature range is 17 ± 1 kJ/mol. The ESPT rate constant of QCy7 forming an ion pair (k_{PT}), at 150 K is about⁶⁰ $2 \times 10^9 \text{ s}^{-1}$; this is twice that of the hopping rate in ice. If the forward and reverse reaction rates are of the same magnitude at 150 K, then the ion-pair population should be quite large at short times of a few nanoseconds, limited by the excited-state lifetimes of both ROH* and RO-* forms of QCy7. The hopping rate at even lower temperatures $T < 150$ K decreases further, as expected from the large activation energy of 17 kJ/mol, whereas the forward reaction rate decreases with a much smaller activation energy of 10.5 kJ/mol. At such low temperatures, k_{PT} decreases more slowly than the proton hopping rate and thus the formation of RO- and a hydrated proton removed by at least two water molecules decreases. At lower temperatures, $110 < T < 150$ K, the hopping time will be much longer than the lifetime of both ROH and RO- excited states (a few nanoseconds), and therefore, the ion-pair spectrum is dominant. As seen in Figure 2a,b, the RO-*...H₃O⁺ ion-pair spectrum of QCy9 is clearly seen over this temperature range. At $T < 112$ K, the ESPT rate is larger than the $k_r + k_{\text{nr}}$ values for ROH* and the efficiency of ESPT in forming the ion pair is still high. The ESPT rate of QCy9 in D₂O ice is slower by at least a factor of 2. The ESPT rate is comparable to k_r and the steady-state emission spectrum consists of the ROH* and RO-*...H₃O⁺ bands of equal intensity. In short, at $T < 150$ K we attribute the red emission band at about 620 nm to the intermediate product of the ESPT process, namely, the RO-*...H₃O⁺ ion pair. To observe the ion-pair intermediate, the rate constants of generation and dissociation of the ion pair must be balanced in such a way that its population will be large in comparison to those of the ROH* and free RO- forms.

SUMMARY AND CONCLUSIONS

In this article we investigated the photoprotolytic process of a photoacid in H₂O and D₂O. We focused our attention on identifying an intermediate product in the excited-state proton transfer to the solvent. Scheme 2 shows the suggested photoprotolytic mechanism of the ESPT process at long times. The concentration of the intermediate depends on four rate constants. When the ESPT rate constant is small compared to the intermediate dissociation rate, it is hopeless to find such an intermediate under neutral-pH conditions.

Previously, we looked for a spectroscopic signature of an ion-pair intermediate RO-*...H₃O⁺ in the femtosecond time-resolved pump–probe spectroscopy of a common photoacid, the 8-hydroxypyrene-1,3,6-trisulfonate (HPTS) whose pK_a^* (≈ 1.3) is rather large and the ESPT rate constant, $k_{\text{PT}} = 10^{10} \text{ s}^{-1}$, is small. For HPTS we found a short transient absorption component at ~ 540 nm with $\tau \sim 3$ ps, which we assign to the ion-pair product. Further studies by Fayer and co-workers⁹ assign this time component in HPTS pump–probe to a slow charge rearrangement that occurs in the excited state of the ROH* form of the photoacid.

In the current study, we used steady-state emission, time-resolved emission and pump–probe spectroscopy to further explore the photoacids photoprotolytic mechanism. The ESPT rate of QCy7 is large⁶⁰ ($k_{\text{PT}} \sim 1.25 \times 10^{12} \text{ s}^{-1}$) and the ESPT rate QCy9 is even larger ($k_{\text{PT}} \sim 10^{13} \text{ s}^{-1}$). Thus, within ~ 200 fs the ROH* form of QCy9 dissociates¹⁹ and only one-tenth of its initial excited-state concentration remains. Therefore, the transient spectra at $t > 0.2$ ps are mainly those of the RO-* form of the photoacid. If Scheme 2 applies and the photoprotolytic intermediate is an ion-pair complex, then the large

Coulomb interaction of RO-* with the hydronium ion may be shifting the electronic levels involved in the transient spectra. This was indeed observed in the current study. The transient pump–probe spectra of QCy9 in water shown in Figure 6c over the time range 0.35–3.8 ps and for QCy9 in D₂O in Figure S7 in the Supporting Information show two absorption bands and two emission bands. We assign one emission band at 630 nm and one absorption band at 575 nm to the RO-*...H₃O⁺ contact ion-pair intermediate. The final product, RO-* and the far-removed hydronium–water complex RO-* + H₃O⁺, show an absorption band of RO-* at 585 nm and an emission band at 715 nm. Thus, the QCy9 transient pump–probe spectra at short times provide evidence for the existence of an ion-pair RO-*...H₃O⁺ as an intermediate product of the photoprotolytic process of photoacids that transfer a proton to solvents like water or alcohols. Another result that explains the position of the emission band of the ion pair of QCy9 and QCy7 in H₂O and D₂O comes from the low-temperature steady-state emission measurements shown in Figure 2 for QCy9 and Figure S1 in the Supporting Information for QCy7 in both water and ice. At temperatures below 165 K, the emission spectra of both QCy9 and QCy7 show an abrupt change in the spectral position of the RO-* emission band in both H₂O and D₂O samples. The RO-* emission band shifts from the high-temperature position at ~ 700 nm to about 630 nm. We assign the 700 nm band to free RO-* and a far-removed proton, and the band at 630 nm to the ion-pair complex RO-*...H₃O⁺. We also find these two emission-band positions in the transient spectra measured in the pump–probe experiments of QCy9 shown in Figure 6c and Figure S4 (Supporting Information).

ASSOCIATED CONTENT

Supporting Information

QCy7 molecular scheme, steady-state emission of QCy7, fluorescence up-conversion signals of QCy9 in a slightly acidified D₂O solution, TCSPC measurements of QCy9 in TCA acid, pump–probe transient spectra and analysis by log-normal line shape functions, curcumin molecular scheme. This material is available free-of-charge via the Internet at <http://pubs.acs.org>

AUTHOR INFORMATION

Corresponding Author

*D. Huppert: e-mail, huppert@tulip.tau.ac.il; phone, 972-3-6407012; fax, 972-3-6407491.

Notes

The authors declare no competing financial interest.

ACKNOWLEDGMENTS

This work was supported by grants from the James-Franck German-Israeli Program in Laser-Matter Interaction and by the Israel Science Foundation.

REFERENCES

- Ireland, J. F.; Wyatt, P. A. Acid-Base Properties of Electronically Excited States of Organic Molecules. *Adv. Phys. Org. Chem.* **1976**, 12, 131–221.
- Gutman, M.; Nachliel, E. The Dynamic Aspects of Proton Transfer Processes. *Biochem. Biophys. Acta* **1990**, 1015, 391–414.
- Tolbert, L. M.; Solntsev, K. M. Excited-State Proton Transfer: From Constrained Systems to “Super” Photoacids to Superfast Proton Transfer. *Acc. Chem. Res.* **2002**, 35, 19–27.

- (4) Rini, M.; Magnes, B. Z.; Pines, E.; Nibbering, E. T. Real-Time Observation of Bimodal Proton Transfer in Acid-Base Pairs in Water. *J. Science* **2003**, *301*, 349–352.
- (5) Mohammed, O. F.; Pines, D.; Dreyer, J.; Pines, E.; Nibbering, E. T. Sequential Proton Transfer Through Water Bridges in Acid-Base Reactions. *J. Science* **2005**, *310*, 83–86.
- (6) Tran-Thi, T. H.; Gustavsson, T.; Prayer, C.; Pommeret, S.; Hynes, J. T. Primary Ultrafast Events Preceding the Photoinduced Proton Transfer from Pyranine to Water. *Chem. Phys. Lett.* **2000**, *329*, 421–430.
- (7) Agmon, N. Elementary Steps in Excited-State Proton Transfer. *J. Phys. Chem. A* **2005**, *109*, 13–35.
- (8) Spry, D. B.; Fayer, M. D. Charge Redistribution and Photoacidity: Neutral Versus Cationic Photoacids. *J. Chem. Phys.* **2008**, *128*, 084508-1–084508-9.
- (9) Spry, D.; Goun, A.; Fayer, M. Deprotonation Dynamics and Stokes Shift of Pyranine (HPTS). *J. Phys. Chem. A* **2007**, *111*, 230–237.
- (10) Siwick, B. J.; Cox, M. J.; Bakker, H. J. Long-Range Proton Transfer in Aqueous Acid–Base Reactions. *J. Phys. Chem. B* **2008**, *112*, 378–389.
- (11) Mohammed, O. F.; Pines, D.; Nibbering, E. T. J.; Pines, E. Base-Induced Solvent Switches in Acid–Base Reactions. *Angew. Chem. Int. Ed.* **2007**, *46*, 1458–1461.
- (12) Mondal, S. K.; Sahu, K.; Sen, P.; Roy, D.; Ghosh, S.; Bhattacharyya, K. Excited State Proton Transfer of Pyranine in a γ -cyclodextrin Cavity. *Chem. Phys. Lett.* **2005**, *412*, 228–234.
- (13) Prasun, M. K.; Samanta, A. Evidence of Ground-State Proton-Transfer Reaction of 3-Hydroxyflavone in Neutral Alcoholic Solvents. *J. Phys. Chem. A* **2003**, *107*, 6334–6339.
- (14) Bhattacharya, B.; Samanta, A. Excited-State Proton-Transfer Dynamics of 7-Hydroxyquinoline in Room Temperature Ionic Liquids. *J. Phys. Chem. B* **2008**, *112*, 10101–10106.
- (15) Pérez Lustres, J. L.; Kovalenko, S. A.; Mosquera, M.; Senyushkina, T.; Flasche, W.; Ernsting, N. P. Ultrafast Solvation of N-Methyl-6-Quinolone Probes Local IR Spectrum. *Angew. Chem., Int. Ed.* **2005**, *44*, S635–S639.
- (16) Pérez -Lustres, J.; Rodriguez-Prieto, F.; Mosquera, M.; Senyushkina, T.; Ernsting, N.; Kovalenko, S. Ultrafast Proton Transfer to Solvent: Molecularity and Intermediates from Solvation-and Diffusion-Controlled Regimes. *J. Am. Chem. Soc.* **2007**, *129*, 5408–5418.
- (17) Karton-Lifshin, N.; Segal, E.; Omer, L.; Portnoy, M.; Satchi-Fainaro, R.; Shabat, D. A unique paradigm for a Turn-ON near-infrared cyanine-based probe: Noninvasive intravital optical imaging of hydrogen peroxide. *J. Am. Chem. Soc.* **2011**, *133* (28), 10960–10965.
- (18) Karton-Lifshin, N.; Albertazzi, L.; Bendikov, M.; Baran, P. S.; Shabat, D. “Donor–Two-Acceptor” Dye Design: A Distinct Gateway to NIR Fluorescence. *J. Am. Chem. Soc.* **2012**, *134* (50), 20412–20420.
- (19) Simkovitch, R.; Karton-Lifshin, N.; Shomer, S.; Shabat, D.; Huppert, D. Ultrafast Excited-State Proton Transfer to the Solvent Occurs on a Hundred-Femtosecond Time-Scale. *J. Phys. Chem. A* **2013**, *117*, 3405–3413.
- (20) Pines, E.; Huppert, D.; Agmon, N. Geminate Recombination in Excited State Proton Transfer Reaction: Numerical Solution of the Debye Smoluchowski Equation with Back Reaction and Comparison with Experimental Results. *J. Chem. Phys.* **1988**, *88*, 5620–5630.
- (21) Agmon, N.; Pines, E.; Huppert, D. Geminate Recombination in Proton Transfer Reactions. II. Comparison of Diffusional and Kinetic Schemes. *J. Chem. Phys.* **1988**, *88*, 5631–5638.
- (22) Debye, P. Reaction Rates in Ionic Solutions. *Trans. Electrochem. Soc.* **1942**, *82*, 265–272.
- (23) Collins, F. C.; Kimball, G. E. Diffusion-Controlled Reaction Rates. *J. Colloid Sci.* **1949**, *4*, 425–437.
- (24) Eigen, M. Proton Transfer, Acid-Base Catalysis, and Enzymatic Hydrolysis. Part I: Elementary Processes. *Angew. Chem., Int. Ed. Engl.* **1964**, *3*, 1–19.
- (25) Weller, A. Fast Reactions of Excited Molecules. *Prog. React. Kinet.* **1961**, *1*, 187–214.
- (26) Leiderman, P.; Genosar, L.; Huppert, D. Excited-State Proton Transfer: Indication of Three Steps in the Dissociation and Recombination Process. *J. Phys. Chem. A* **2005**, *109*, 5965–5977.
- (27) Gepshtein, R.; Leiderman, P.; Genosar, L.; Huppert, D. Testing the Three Step Excited State Proton Transfer Model by the Effect of an Excess Proton. *J. Phys. Chem. A* **2005**, *109*, 9674–9684.
- (28) Iftimie, R.; Tremblay, M.; Thomas, V.; Hetu, S.; de Lasalle, F.; Rivard, U. Moderately Strong Phenols Dissociate by Forming an Ion-Pair Kinetic Intermediate. *J. Phys. Chem. A* **2013**.
- (29) Uritski, A.; Presiado, I.; Erez, Y.; Gepshtein, R.; Huppert, D. Temperature Dependence of Proton Diffusion in Ih Ice. *J. Phys. Chem. C* **2009**, *113*, 10285–10296.
- (30) Uritski, A.; Presiado, I.; Huppert, D. Isotope Effect of Proton/Deuteron Diffusion Constant in Ice. *Isr. J. Chem.* **2009**, *49*, 235–250.
- (31) Uritski, A.; Presiado, I.; Erez, Y.; Gepshtein, R.; Huppert, D. Classification of Acids and Acidities in Ih Ice II: Reversible Photoacids As a Probe for Proton Concentration. *J. Phys. Chem. C* **2009**, *113*, 12901–12910.
- (32) Gol'danshlii, V. I.; Trakhtenberg, L. I.; Fleurov, V. N. *Tunnelling Phenomena in Chemical Physics*; Gordon and Breach: Philadelphia, PA, 1989.
- (33) Uritski, A.; Presiado, I.; Erez, Y.; Gepshtein, R.; Huppert, D. Classification of Acids and Acidities in Ih Ice II: Reversible Photoacids As a Probe for Proton Concentration. *J. Phys. Chem. C* **2009**, *113*, 12901–12910.
- (34) Presiado, I.; Lal, J.; Mamontov, E.; Kolesnikov, S.; Huppert, D. Fast Proton Hopping Detection in Ice Ih by Quasi-Elastic Neutron Scattering. *J. Phys. Chem. C* **2011**, *115*, 10245–10251.
- (35) Petrenko, V. F.; Whitworth, R. W. *The Physics of Ice*; Oxford University Press: Oxford, U.K., 1999.
- (36) Takei, I.; Maeno, N. Dielectric properties of single crystals of HCl-doped ice. *J. Phys. Chem.* **1984**, *81*, 6186–6190.
- (37) Takei, I.; Maeno, N. Electric characteristics of point defects in HCl-doped ice. *J. Phys. (Paris)* **1987**, *48*, Colloque C1, 121–126.
- (38) Presiado, I.; Lal, J.; Mamontov, E.; Kolesnikov, S.; Huppert, D. Fast Proton Hopping Detection in Ice Ih by Quasi-Elastic Neutron Scattering. *J. Phys. Chem. C* **2011**, *115*, 10245–10251.
- (39) Simkovitch, R.; Shomer, S.; Gepshtein, R.; Shabat, D.; Huppert, D. Temperature Dependence of the Excited-State Proton-Transfer Reaction of Quinone-Cyanin-7. *J. Phys. Chem. A* **2013**, *117*, 3925–3934.
- (40) Agmon, N.; Pines, E.; Huppert, D. Geminate Recombination in proton-transfer Reactions. II. Comparison of Diffusional and Kinetic Schemes. *J. Chem. Phys.* **1988**, *88*, 5631–5638.
- (41) Fraser, R.; Suzuki, E.; Dekker, M. *Biological Applications. Spectral analysis: methods and techniques*; Dekker: New York, 1970; pp 171–211.
- (42) Collie, C.; Hasted, J.; Ritson, D. The Dielectric Properties of Water and Heavy Water. *Proc. Phys. Soc.* **1948**, *60*, 145.
- (43) Chen, W.; Braiman, M. S. Kinetic Analysis of Time-Resolved Infrared Difference Spectra of the L and M Intermediates of Bacteriorhodopsin*. *Photochem. Photobiol.* **1991**, *54*, 905–910.
- (44) Zundel, G. In *The Hydrogen Bond, Recent Developments in Theory and Experiments*; Schuster, P.; Zundel, G.; Sandorfy, C., Eds.; North-Holland: Amsterdam, 1976; pp 687–766.
- (45) Zundel, G. Hydrogen Bonds with Large Proton Polarizability and Proton Transfer Processes in Electrochemistry and Biology. *Adv. Chem. Phys.* **2000**, *111*, 1–217.
- (46) Ghosh, R.; Mondal, J. A.; Palit, D. K. Ultrafast Dynamics of the Excited States of Curcumin in Solution. *J. Phys. Chem. B* **2010**, *114*, 12129–12143.
- (47) Akulov, K.; Simkovitch, R.; Erez, Y.; Gepshtein, R.; Schwartz, T.; Huppert, D. Acid Effect on Photobase Properties of Curcumin. *J. Phys. Chem. A* **2014**, *118*, 2470–2479.
- (48) Erez, Y.; Simkovitch, R.; Shomer, S.; Gepshtein, R.; Huppert, D. The Effect of Acid on the UV-Visible Absorption and Emission Properties of Curcumin. *J. Phys. Chem. A* **2014**, *118*, 872–884.
- (49) Erez, Y.; Presiado, I.; Gepshtein, R.; Huppert, D. The Effect of a Mild Base on Curcumin in Methanol and Ethanol. *J. Phys. Chem. A* **2012**, *116*, 2039–2048.
- (50) Horng, M.; Gardecki, J.; Papazyan, A.; Maroncelli, M. Subpicosecond Measurements of Polar Solvation Dynamics: Coumarin 153 Revisited. *J. Phys. Chem. A* **1995**, *99*, 17311–17337.

- (51) Stoyanov, E. S.; Kim, K.-C.; Reed, C. A. The Nature of the H₃O⁺ Hydronium Ion in Benzene and Chlorinated Hydrocarbon Solvents. Conditions of Existence and Reinterpretation of Infrared Data. *J. Am. Chem. Soc.* **2006**, *128*, 1948–1958.
- (52) Stoyanov, E. S.; Stoyanova, I. V.; Reed, C. A. The unique nature of H⁺ in water. *Chem. Sci.* **2011**, *2*, 462–472.
- (53) Mohammed, O. F.; Pines, D.; Dreyer, J.; Pines, E.; Nibbering, E. T. Sequential Proton Transfer through Water Bridges in Acid-Base Reactions. *Science* **2005**, *310*, 83–86.
- (54) Sigalov, M. V.; Kalish, N.; Carmeli, B.; Pines, D.; Pines, E. Probing Small Protonated Water Clusters in Acetonitrile Solutions by ¹H NMR. *Z. Phys. Chem. (Muenchen, Ger.)* **2013**, *227*, 983–1007.
- (55) Kalish, N. B.; Shandalov, E.; Kharlanov, V.; Pines, D.; Pines, E. Apparent Stoichiometry of Water in Proton Hydration and Proton Dehydration Reactions in CH₃CN/H₂O Solutions. *J. Phys. Chem. A* **2011**, *115*, 4063–4075.
- (56) Veiga-Gutiérrez, M.; Brenlla, A.; Carreira Blanco, C.; Fernández, B.; Kovalenko, S. A.; Rodríguez-Prieto, F.; Mosquera, M.; Lustres, J. L. P. Dissociation of a Strong Acid in Neat Solvents: Diffusion is Observed After Reversible Proton Ejection Inside the Solvent Shell. *J. Phys. Chem. B* **2013**, *117*, 14065–14078.
- (57) Iftimie, R.; Tremblay, M.; Thomas, V.; Hétu, S.; de Lasalle, F.; Rivard, U. Moderately Strong Phenols Dissociate by Forming an Ion-Pair Kinetic Intermediate. *J. Phys. Chem. A* **2013**, *117*, 13976–13987.
- (58) Liu, W.; Han, F.; Smith, C.; Fang, C. Ultrafast Conformational Dynamics of Pyranine during Excited State Proton Transfer in Aqueous Solution Revealed by Femtosecond Stimulated Raman Spectroscopy. *J. Phys. Chem. B* **2012**, *116*, 10535–10550.
- (59) Han, F.; Liu, W.; Fang, C. Excited-State Proton Transfer of Photoexcited Pyranine in Water Observed by Femtosecond Stimulated Raman Spectroscopy. *Chem. Phys.* **2013**, *422*, 204–219.
- (60) Karton-Lifshin, N.; Presiado, I.; Erez, Y.; Gepshtein, R.; Shabat, D.; Huppert, D. Ultrafast Excited-State Intermolecular Proton Transfer of Cyanine Fluorochrome Dyes. *J. Phys. Chem. A* **2011**, *116*, 85–92.